

Statistical Methods for the Search of Sterile Neutrinos

Matteo Agostini* and Birgit Neumair†

Physik Department, Technische Universität München, Germany

(Dated: September 11, 2022)

The statistical methods applied to search for short-baseline neutrino oscillations induced by a sterile neutrino with mass at the eV scale are reviewed and compared. The comparison is performed under limit setting and signal discovery scenarios, considering both when an oscillation would enhance the neutrino interaction rate in the detector and when it would reduce it. The sensitivity of the experiments and the confidence regions extracted for specific data sets are found to change significantly according to the test statistic used for the hypothesis testing. The most general test statistic does not make assumptions on the value of the parameters of interest for the analysis, while the others restrict the allowed parameter space. The restriction of the parameter space could lead to miss a signal or, vice versa, to claim a discovery when this is not statistically significant. Similar issues are found also when the validity of Wilks' theorem is assumed. A standardized analysis approach based on the most general kind of hypothesis test is proposed.

I. INTRODUCTION

A vast experimental program has been mounted in the last decade to search for a new elementary particle named sterile neutrino [1]. The sterile neutrino is a particular type of neutrino that does not interact through the weak force. Since B. Pontecorvo postulated its existence in 1967 [2], the sterile neutrino has become increasingly popular and its existence is nowadays often invoked to explain the mysterious origin of neutrino masses and dark matter [3]. The discovery of sterile neutrinos would hence be a milestone towards the development of new theories beyond the Standard Model, with deep repercussions in particle physics and cosmology.

The phenomenology of sterile neutrinos depends on their hypothetical mass value. The main target of the ongoing experimental efforts is sterile neutrinos with a mass of the order of the eV, whose existence has been hinted at by various experiments [4–6] and is still under debate [1, 7]. The statistical data treatment for these kind of searches presents various challenges and has not been standardized yet. Currently, different statistical methods are used in the field, each addressing a different statistical question, and thus providing different results. This situation prevents a direct comparison of the performance of the experiments and of their outcome. In addition, approximations often adopted in the statistical analysis can lead to significantly inaccurate results.

In this article we review the statistical methods used in the search for sterile neutrinos at the eV mass scale, expanding the discussion of Refs. [8–10] and performing a comprehensive comparison of the analysis approaches in scenarios with and without a signal. Section II describes the phenomenology of eV-mass sterile neutrinos, the signature sought after by the experiments, and the features of two toy experiments that are used in this ar-

ticle to compare the analysis techniques. Section III reviews the statistical methods and concepts used in the field. The performance of the different methods are discussed in Section IV and V. Finally, in Section VI, the methods are compared and a reference analysis procedure to present new experimental results is proposed.

II. PHENOMENOLOGY AND EXPERIMENTS

Neutrinos of three different flavours have been observed: the electron (ν_e), the muon (ν_μ) and the tau neutrino (ν_τ) [11]. These standard neutrinos can be detected by experiments because they interact through the weak force. Neutrinos can change flavor as they move through space. This phenomenon, called neutrino flavour oscillation, is possible because the standard neutrinos do not have a fixed mass but are rather a quantum-mechanical superposition of different mass eigenstates (i.e. ν_1 , ν_2 , and ν_3), each associated to a distinct mass eigenvalue (m_1 , m_2 and m_3).

A sterile neutrino (ν_s) would not interact through the weak force and cannot be directly detected. However its existence would affect the standard neutrino oscillations in two ways. Firstly, a standard neutrino could oscillate into an undetectable sterile neutrino, leading to a reduction of the observed event rate within the detector. Secondly, the mass eigenstate (ν_4 with mass m_4) primarily associated to the sterile neutrino would enhance the transformation probability between standard neutrinos, leading to the detection of a neutrino flavor that is not emitted by the source. The experiments looking for a reduction of the interaction rate are called “disappearance” experiments while the ones seeking for an enhanced neutrino conversion are called “appearance” experiments. In principle, more than one sterile neutrino with mass at the eV scale could exist. In this work we will focus on the scenario in which there is only one eV-mass sterile neutrino.

The current-generation sterile-neutrino experiments are designed to search for neutrino oscillations at a short

* matteo.agostini@tum.de

† birgit.neumair@ph.tum.de

distance from the neutrino source, where the effect of neutrino oscillations is expected to be negligible unless an eV-mass sterile neutrino exists. The oscillation probability expected by these so-called short-baseline experiments can be approximated by:

$$P(\nu_\alpha \rightarrow \nu_\alpha) = 1 - \sin^2(2\theta_{\alpha\alpha}) \sin^2\left(k \cdot \Delta m^2 \cdot \frac{L}{E}\right) \quad (1)$$

$$P(\nu_\alpha \rightarrow \nu_\beta) = \sin^2(2\theta_{\alpha\beta}) \sin^2\left(k \cdot \Delta m^2 \cdot \frac{L}{E}\right) \quad (2)$$

where $P(\nu_\alpha \rightarrow \nu_\alpha)$ is the survival probability for a specific neutrino of flavor α and $P(\nu_\alpha \rightarrow \nu_\beta)$ is the probability for a neutrino of flavor α to transform into the flavor β (ν_α and ν_β indicate any of the standard neutrino flavors, i.e.: ν_e, ν_μ and ν_τ). The mixing angles (i.e. $\theta_{\alpha\alpha}$ and $\theta_{\alpha\beta}$) and the difference between the squared mass eigenvalues (i.e. $\Delta m^2 = m_4^2 - m_1^2$) are physical constants. The experiments aim at extracting these constants from the measurement of the oscillation probability as a function of the distance travelled by the neutrino before its interaction (L) and its initial energy (E). The maximum value of the oscillation probability is proportional to $\sin^2(2\theta)$ that acts as a scaling factor, while the modulation of the probability is determined by Δm^2 . The constant $k = 1.27 \text{ MeV}/\text{eV}^2/\text{m}$ applies when Δm^2 is expressed in eV^2 , L in meters and E in MeV. The modulation of the oscillation as a function of L/E is shown in in FIG. 1a for a selection of Δm^2 values.

The features of various short-baseline experiments are summarized in TABLE I. Different kinds of neutrino sources and detection technologies are used. The most common neutrino sources are nuclear reactors (producing electron anti-neutrinos up to 10 MeV), radioactive sources (electron neutrinos and anti-neutrinos up to a few MeV), and particle accelerators (muon neutrinos and anti-neutrinos up to several GeV). The detector designs are very different, but they mostly rely on scintillating materials and light detectors, or on liquid-argon time projection chambers [1].

In order to extract the sterile neutrino parameters, both L and E must be reconstructed for each detected neutrino. The oscillation baseline L is well defined as either it is much larger than the dimensions of the source and the detector – as in accelerator-based experiments – or the source is relatively compact and the detector is capable of reconstructing the position of an event – as in experiments with radioactive isotopes or reactors. The reconstruction of the event position is achieved with the physical segmentation of the detector and/or with advanced analysis techniques based on the properties of the scintillation or ionization signal.

The strategy used to reconstruct E varies according to the primary channel through which neutrinos interact in the detector. Experiments using low energy anti-neutrinos can measure E through a calorimetric approach thanks to the fact that anti-neutrinos interact via inverse beta decay and their energy is entirely absorbed within

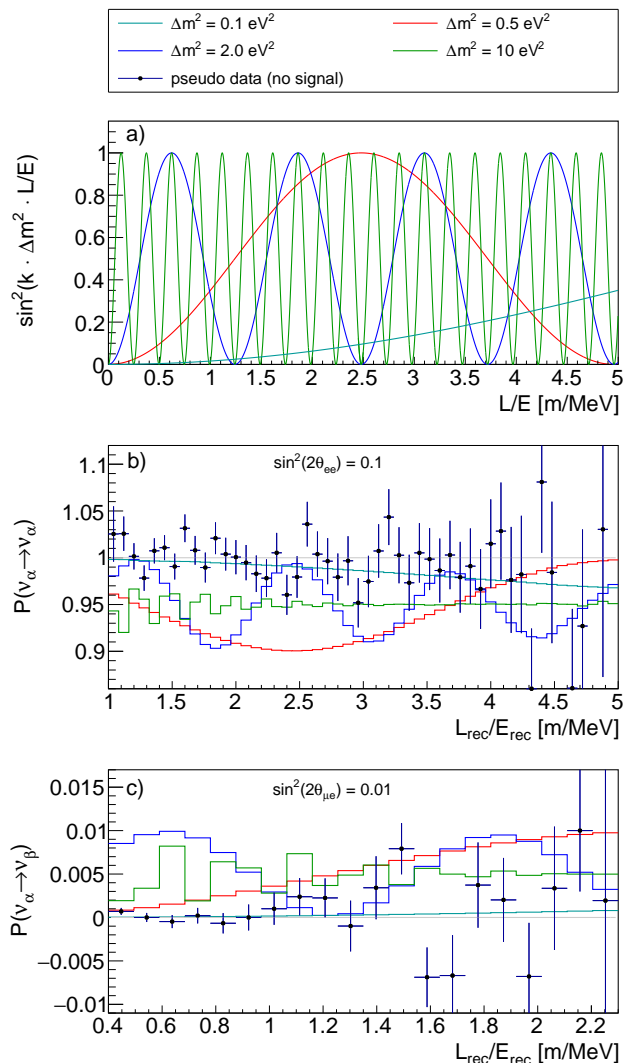


FIG. 1. (a) Normalized probability of a neutrino flavor oscillation as a function of L/E for different Δm^2 values. The absolute probability is given by the product between the plotted normalized probability and $\sin^2(2\theta)$. (b and c) Probability of neutrino oscillations as a function of $L_{\text{rec}}/E_{\text{rec}}$ for two toy experiments searching for a disappearance (b) and an appearance (c) signal. The probabilities are shown assuming the existence of sterile neutrinos at various possible $\sin^2(2\theta)$ and Δm^2 values. The reconstructed probability from pseudo-data generated with Monte Carlo simulations under the hypothesis that there are no sterile neutrinos are also shown. The binning reflects the typical experimental resolutions on L_{rec} and E_{rec} . The error bars account for the statistical uncertainties.

the detector. In experiments with high energy neutrinos interacting through charge-current quasi-elastic reactions, E is estimated from the kinematic of the particles produced in the interaction. Some experiments use neutrinos that interact through electron scattering and release only a random fraction of their energy inside the detector. In this cases the energy cannot be accurately reconstructed and monoenergetic neutrino sources are typically used. In the following we will use L_{rec} and

TABLE I. Features and parameters of a selection of short-baseline experiments grouped according to the source of neutrinos. The kind of neutrinos emitted by the source and those detected by the experiment are shown in the third column. For each experiment the accessible range of L_{rec} , E_{rec} , and $L_{\text{rec}}/E_{\text{rec}}$ are given along with the binning used to analyze the data and the expected number of neutrino and background events. The number of neutrino events is given assuming no oscillations in disappearance experiments and the flavor transformation of all neutrinos for appearance experiments. Absolute resolutions on the reconstructed baseline and energy (σ_L and σ_E) are quoted for the mean value of L_{rec} and E_{rec} . The parameters quoted in this table are sometimes effective or approximated quantities and are intended to give an idea of the signal expected in each experiment. The last two rows show the parameters of two toy experiments used in this work to compare statistical methods. The toy experiments have parameters typical of disappearance searches based on nuclear reactors and appearance searches based on accelerators.

	Detection technology	Sought-after oscillation	L_{rec} [m] range	σ_L	E_{rec} [MeV] range	σ_E	$L_{\text{rec}}/E_{\text{rec}}$ range	binning $L_{\text{rec}} \times E_{\text{rec}}$	\bar{N}_s	\bar{N}_b
<i>Experiments with neutrinos from nuclear reactors:</i>										
DANSS [12]	Gd-coated plastic scintillator	$\bar{\nu}_e \rightarrow \bar{\nu}_e$	11–13	0.2	1–7	0.6	1.5–13	3×24	10 ⁶	10 ⁴
NEOS [13]	Gd-loaded liquid scintillator	$\bar{\nu}_e \rightarrow \bar{\nu}_e$	24	1	1–7	0.1	3.5–24	1×60	10 ⁵	10 ⁴
NEUTRINO-4 [14]	Gd-loaded liquid scintillator	$\bar{\nu}_e \rightarrow \bar{\nu}_e$	6–12	0.2	1–6	0.3	1–12	24×9	10 ⁵	10 ⁶
PROSPECT [15]	Li-loaded liquid scintillator	$\bar{\nu}_e \rightarrow \bar{\nu}_e$	7–9	0.15	1–7	0.1	1–9	6×16	10 ⁴	10 ⁴
SoLid [16]	Li-coated PVT scintillator	$\bar{\nu}_e \rightarrow \bar{\nu}_e$	6–9	0.05	1–7	0.2	1–9		10 ⁵	10 ⁵
STEREO [17]	Gd-loaded liquid scintillator	$\bar{\nu}_e \rightarrow \bar{\nu}_e$	9–11	0.3	2–7	0.1	1.3–5.5	6×11	10 ⁴	10 ⁴
<i>Experiments with neutrinos from radioactive sources:</i>										
BEST [18]	Ga radiochemical	$\nu_e \rightarrow \nu_e$	0.1–1	0.6	0.4–1.4	–	0.1–2.5		10 ⁴	10 ²
SOX [19, 20]	liquid scintillator	$\bar{\nu}_e \rightarrow \bar{\nu}_e$	4–12	0.15	2–3	0.1	1.3–6.5		10 ⁴	10 ²
<i>Experiments with neutrinos from particle accelerators:</i>										
JSNS ² [21]	Gd-loaded liquid scintillator	$\bar{\nu}_\mu \rightarrow \bar{\nu}_e$	24	5	10–50	5	0.5–2.5		10 ⁵	10 ²
LSND [4]	liquid scintillator	$\bar{\nu}_\mu \rightarrow \bar{\nu}_e$	30	10	20–60	3	0.5–1.5	1×10	10 ⁴	30
MiniBooNE [22]	mineral oil	$\nu_\mu \rightarrow \nu_e$ $\bar{\nu}_\mu \rightarrow \bar{\nu}_e$	500	50	200–3000	20	0.2–2.5	1×11	10 ⁵	10 ³
SBN@FNAL [23]	Ar time projection chamber	$\nu_\mu \rightarrow \nu_e$	110–600	50	200–3000	15	0.1–3		10 ⁵	10 ³
<i>Toy experiments:</i>										
Disappearance		$\bar{\nu}_e \rightarrow \bar{\nu}_e$	7–10	0.5	2–7	5	1–5	6×10	10 ⁵	10 ⁴
Appearance		$\nu_\mu \rightarrow \nu_e$	500–550	50	200–1200	10	0.4–2.4	1×20	10 ⁵	10 ³

E_{rec} to refer to the reconstructed value of baseline and energy.

TABLE I shows for each experiment range and resolution of L_{rec} and E_{rec} . In order to maximize the sensitivity to sterile neutrino masses at the eV-scale, the experiments are designed such to be sensitive to $L_{\text{rec}}/E_{\text{rec}}$ values of the order of 1 m/MeV. The experiments can thus observe multiple oscillations within the detector for Δm^2 values at the eV scale. As the sought-after signal is similar among the experiments, the issues and challenges related to the statistical data treatment are the same.

The analysis of an experiment can exploit two complementary pieces of information. When the neutrino energy spectrum, flux and cross section are accurately known, the integral number of neutrino interactions expected within the detector can be computed for a given oscillation hypothesis and compared with the observed one. This approach is often called “rate” analysis. Alternatively, the relative change of rate as a function of the interaction position and neutrino energy can be com-

pared with the expectations under different oscillation hypotheses, leaving unconstrained the integral number of events. This second approach is known as “shape” analysis. Rate and shape analysis are used simultaneously to maximize the experimental sensitivity, however they are affected by different systematic uncertainties and for a specific experiment only one of the two might be relevant. In the following we will discuss these two analyses separately. Results for a specific experiment can be estimated by interpolating between these two extreme cases. Experiments based on nuclear reactors often use the so-called “ratio” method [17], in which the energy spectrum measured in a given part of the detector is normalized against what observed in a reference section. The ratio method has features similar to the shape analysis and it is not explicitly considered in the following.

Two toy experiments are used in this work to compare different analysis techniques. The first one is an example of disappearance experiment representative of the projects using nuclear reactors or radioactive isotopes

as anti-neutrino source. In these experiments, the electron anti-neutrinos partially convert into sterile neutrinos with different probabilities as a function of L_{rec} and E_{rec} . The anti-neutrino energy spectrum is considered between 2 to 7 MeV and the range of oscillation baselines accessible by the experiment is from 7 to 10 m ($L_{\text{rec}}/E_{\text{rec}} = 1\text{--}5\text{ m/MeV}$ with a resolution varying between 5 and 10%). The second toy experiment is an example of appearance experiment in which muon neutrinos transform into electron neutrinos with a probability enhanced by the existence of sterile neutrinos. In this case, typical for experiments based on particle accelerators, the neutrino energy varies between 200 and 1200 MeV and the oscillation baseline between 500 and 550 m ($L_{\text{rec}}/E_{\text{rec}} = 0.4\text{--}2.4\text{ m/MeV}$ with a resolution varying between 10 and 25%).

The toy disappearance experiments can observe an oscillatory pattern in the event rate as a function of both energy and baseline, whereas the appearance experiment can observe it only in energy as the baseline can be regarded as fixed. The energy distribution of both the neutrinos emitted by the source and the background events is assumed to be flat. This is not the case in real experiments where the initial neutrino energy is peaked at some value and the background spectrum depends on the background sources. However this approximation does not affect the study reported in this work. The experimental parameters of our toy experiments, including the number of signal and background events, are summarized in the last two rows of TABLE I. The uncertainties on the signal and background rates are assumed to have the realistic values of 10% and 5% for the appearance experiment, and of 2% both for the signal and background rate in the disappearance experiment.

An example of the oscillation probability reconstructed from our toy experiments is shown in FIG. 1b and 1c as a function of $L_{\text{rec}}/E_{\text{rec}}$. The probability is reconstructed from a set of pseudo-data generated with Monte Carlo simulations from a model with no sterile neutrinos. The oscillation probability expected assuming the existence of sterile neutrinos is shown for four mass values ($\Delta m^2 = 0.1, 0.5, 2$ and 10 eV^2). Given the $L_{\text{rec}}/E_{\text{rec}}$ resolution of our toy experiments, an oscillatory pattern can be observed only for Δm^2 of 0.5 and 2 eV^2 . For higher Δm^2 values, the frequency of the oscillation becomes too high and only an integrated reduction of the rate is visible. For smaller Δm^2 values, the oscillation length approaches the full $L_{\text{rec}}/E_{\text{rec}}$ range to which the experiment is sensitive, resulting in a loss of sensitivity. In the appearance experiments the discrimination power among different oscillatory patterns relies only on E_{rec} since L_{rec} is fixed.

In this work we focus on short-baseline experiments. We do not consider other oscillation experiments (e.g. Daya Bay [24], Double Chooz [25], RENO [26], MINOS [27], NOvA [28] and Ice Cube [29]) for which the oscillation probability cannot be approximated by equations (1) and (2) as it is either complicated by the overlap between oscillations driven by multiple mass eigen-

states or by matter effects [7]. We also do not consider approaches that are not based on oscillations such as the study of the cosmological structures [30], the high-precision spectroscopy of beta-decays (e.g. KATRIN [31]), or electron captures (e.g. ECHO [32]). The statistical issues of these searches are different from those of the short-baseline experiments and would require a specific discussion.

III. STATISTICAL METHODS

The goal of the short-baseline experiments is to search for a signal due to a sterile neutrino with mass at the eV-scale by measuring the oscillation probability at different L and E values. The parameters of interest associated to the sterile neutrino are the mixing angle and its mass eigenvalue. However, because of the functional form of equations (1) and (2), the observables of the experiments are a function of angle and mass, i.e.: $\sin^2(2\theta)$ and Δm^2 . In the following we will refer to $\sin^2(2\theta)$ and Δm^2 as the parameters of interest of the analysis.

The role of statistical inference applied to the data from sterile neutrino searches can be divided into four tasks:

1. point estimation: the computation of the most plausible value for $\sin^2(2\theta)$ and Δm^2 ;
2. hypothesis testing: given an hypothesis on the value of $\sin^2(2\theta)$ and Δm^2 , decide whether to accept or reject it in favor of an alternative hypothesis. Among the different tests that can be performed, testing the hypothesis that there is no sterile neutrino signal (i.e. $\sin^2(2\theta) = 0$ or $\Delta m^2 = 0$) is of primary interest for an experiment. Rejecting the no-signal hypothesis is equivalent to claiming the observation of a sterile neutrino signal;
3. interval estimation: construct a set of $\sin^2(2\theta)$ and Δm^2 values that includes the true parameter values at some pre-defined confidence level;
4. goodness of fit: estimate if the data can be described by the model.

The statistical methods applied by sterile neutrino experiments to perform the first three tasks are all based on the likelihood function. The point estimation is carried out using maximum likelihood estimators, i.e. by finding the values of $\sin^2(2\theta)$ and Δm^2 that correspond to the maximum of the likelihood function. The hypothesis testing is based on the ratio of likelihoods. The interval estimation is carried out by inverting a set of likelihood-ratio based hypothesis tests, and grouping the hypotheses that are accepted.

The task related to the goodness-of-fit estimation requires a dedicated discussion. Formally, a goodness-of-fit test is a particular kind of hypothesis test in which the alternative hypothesis is not specified. Such a test is often

used in high-energy physics to verify that the data can be described by the model used for the analysis. Model inaccuracies in sterile neutrino searches can be due, for instance, to an underestimation of the systematic uncertainties related to the detector response or to an incomplete physics theory (e.g. there is more than one sterile neutrino flavour at the eV-mass scale). The source of the inaccuracies should be identified and corrected before performing statistical inference. If the analysis is based on a model that cannot describe the data, the interpretation of the results becomes unclear. A goodness-of-fit test can be carried out assuming the most plausible value of the parameters of the model (i.e. the maximum likelihood estimator for $\sin^2(2\theta)$ and Δm^2) and using for instance a Pearson χ^2 or a “likelihood ratio” test [33].

While the procedures for point estimation and goodness of fit are not controversial, the hypothesis testing differs significantly among the experiments since multiple definitions of the hypotheses are possible. Changing the hypothesis definition does not only affect the outcome of the hypothesis test but also of the interval estimation, which is performed by running a set of hypothesis tests. The comparison of tests based on different hypothesis definitions is the subject of Sections IV, V and VI.

In this section we review the ingredients needed to build the tests and the statistical concepts that will be used in the following. Firstly, we consider the likelihood function and derive a general form that can be applied to all experiments (Section III A). Then we discuss the possible hypothesis definitions and the resulting test statistics (Section III B). The significance of a sterile-neutrino signal is defined in Section III C. Finally, in Section III D we examine the construction of confidence regions and in Section III E the concept of sensitivity.

Bayesian methods have not been applied in the search for sterile neutrinos so far. Even if their usage could be advantageous, we will not consider them in the following to keep the focus on the currently used methods.

A. The Likelihood Function

Short-baseline experiments measure the oscillation baseline and the energy of neutrinos, i.e. a pair of $\{L_{\text{rec}}, E_{\text{rec}}\}$ values for each event. L_{rec} and E_{rec} are random variables whose probability distributions depend on the true value of L and E , as well as on the stochastic processes related to the interaction of the neutrino and its detection. Monte Carlo simulations are hence used to construct the probability distributions of L_{rec} and E_{rec} for a neutrino event given a $\sin^2(2\theta)$ and Δm^2 value, $p_s(L, E | \sin^2(2\theta), \Delta m^2)$, and for a background event, $p_b(L, E)$. Additional quantities are sometimes measured, however they are ultimately used to constrain the background or the systematic uncertainties and can be neglected in this work.

To our knowledge, all the experiments organize the data in histograms and base their analysis on a binned

likelihood function. The use of histograms is motivated by the fact that the number of neutrino events is large, between 10^4 and 10^6 as shown in TABLE I. Binning the data leads to a new set of random variables that are the numbers of observed events in each bin: $N^{\text{obs}} = \{N_{11}^{\text{obs}}, N_{12}^{\text{obs}}, \dots, N_{ij}^{\text{obs}} \dots\}$ where i runs over the L_{rec} bins and j over the E_{rec} bins. Consistently, we indicate with PDF_{ij}^s and PDF_{ij}^b the integral of the probability distribution function for neutrino and background events over each bin:

$$\text{PDF}_{ij}^s = \int_{E, L \in \text{bin}_{ij}} p_s(L, E | \sin^2(2\theta), \Delta m^2) dL dE \quad (3)$$

$$\text{PDF}_{ij}^b = \int_{E, L \in \text{bin}_{ij}} p_b(L, E) dL dE. \quad (4)$$

The generic likelihood function can hence be written as:

$$\mathcal{L}(\sin^2(2\theta), \Delta m^2, N^s, N^b | N^{\text{obs}}) = \prod_{ij} \mathcal{P}(N_{ij}^{\text{obs}} | N^s \cdot \text{PDF}_{ij}^s(\sin^2(2\theta), \Delta m^2) + N^b \cdot \text{PDF}_{ij}^b) \quad (5)$$

where i and j run over L_{rec} and E_{rec} bins, $\mathcal{P}(N | \lambda)$ indicates the Poisson probability of measuring N events given an expectation λ , and N^s and N^b are scaling factors representing the total number of neutrino and background events.

External constraints on the number of neutrino and background events related to auxiliary data are here included as additional multiplicative Gaussian terms:

$$\mathcal{L} \rightarrow \mathcal{L} \cdot \mathcal{G}(\bar{N}^s(\sin^2(2\theta), \Delta m^2) | N^s, \sigma^s) \cdot \mathcal{G}(\bar{N}^b | N^b, \sigma^b) \quad (6)$$

where $\mathcal{G}(\bar{N} | N, \sigma)$ indicates the probability of measuring \bar{N} given a normal distributed variable with mean N and standard deviation σ . It should be noted that the expected number of neutrino counts \bar{N}^s depends on the particular oscillation hypothesis tested. Examples of the likelihood can be found in Appendix A.

While $\sin^2(2\theta)$ and Δm^2 are the parameters of interest of the analysis, N^s and N^b are nuisance parameters. The constraints on these parameters could follow different probability distributions and additional nuisance parameters could also be needed, e.g. to account for systematic uncertainties in the detector response, neutrino source, and event reconstruction efficiency. The actual number of nuisance parameters and the particular form of their constraints in the likelihood does not affect the results of our work. To keep the discussion general, in the following we will indicate with $\boldsymbol{\eta} = \{N_s, N_b, \dots\}$ a generic vector of nuisance parameters. Each parameter has an allowed parameter space, for instance the number of neutrino and background events are bounded to positive real values. The nuisance parameters are hence assumed to be constrained in their allowed parameter space even if not explicitly stated.

The general form of the likelihood given in equation (6) accounts for a simultaneous rate and shape analysis. A pure shape analysis will be emulated by removing the

term accounting for the external constraint on the number of neutrino events. Conversely, a pure rate analysis will be emulated by enlarging the size of the bins in PDF^s and PDF^b up to the point at which there is a single bin and any information on the number of events as a function of L_{rec} or E_{rec} is lost.

B. Hypothesis Testing and Test Statistics

A hypothesis test is a procedure in which two hypotheses are compared [34]. The reference hypothesis is denoted with H_0 (i.e. the null hypothesis) while the alternative hypothesis with H_1 . The procedure specifies for which data sets the decision is made to accept H_0 or, alternatively, to reject H_0 and accept H_1 . Usually a hypothesis test is specified in terms of a test statistic T and a critical region for it. The test statistic is a function of the data that returns a real number. The critical region is the range of test statistic values for which the null hypothesis is rejected in favour of the alternative.

The critical region is chosen such that the test rejects H_0 with a given probability when H_0 is actually true. Such a probability is denoted with α and called the “size” of the test. In the physics community, it is more frequent to quote $1 - \alpha$ and refer to it as the confidence level of the test. For instance, if H_0 is rejected with $\alpha = 5\%$ probability when it is true, the test is said to have 95% confidence level (C.L.). In order to compute the critical threshold in each test, the probability distribution of the test statistic must be known. In our work, the distributions are constructed from large ensembles of pseudo-data sets generated via Monte Carlo methods following the method described in Appendix B.

In sterile neutrino searches an hypothesis is defined by a set of allowed values for $\sin^2(2\theta)$ and Δm^2 . The null hypothesis is defined as:

$$H_0 : \{\sin^2(2\theta), \Delta m^2 : \sin^2(2\theta) = X, \Delta m^2 = Y\} \quad (7)$$

where X and Y are two particular values. Since the mixing angle and the mass eigenvalue are defined as positive real numbers by the theory and $m_4 \geq m_1$, the most general version of the alternative hypothesis is

$$H_1 : \{\sin^2(2\theta), \Delta m^2 : 0 \leq \sin^2(2\theta) \leq 1, \Delta m^2 \geq 0\}. \quad (8)$$

A test based on these two hypotheses leads to a generalized likelihood-ratio test statistic of the form [34]:

$$T = -2 \ln \frac{\sup_{\eta} \mathcal{L}(\sin^2(2\theta) = X, \Delta m^2 = Y, \eta | N^{obs})}{\sup_{\sin^2(2\theta), \Delta m^2, \eta} \mathcal{L}(\sin^2(2\theta), \Delta m^2, \eta | N^{obs})} \quad (9)$$

where the denominator is the maximum of the likelihood for the observed data set over the parameter space allowed for the parameters of interest ($\{\sin^2(2\theta), \Delta m^2\} \in H_1$) and the nuisance parameters. The numerator is instead the maximum of the likelihood in the restricted

space in which $\sin^2(2\theta)$ and Δm^2 are equal to the value specified by H_0 .

If the value of Δm^2 or $\sin^2(2\theta)$ are considered to be known because of theoretical predictions or of a measurement, then the parameter space of the alternative hypothesis can be restricted. Restricting the parameter space is conceptually equivalent to folding into the analysis new assumptions and changes the question addressed by the hypothesis test. Since the question changes, also the outcome of the test can change. The more restrictive is the alternative hypothesis, the more powerful the test will be.

Three tests have been used in the context of sterile neutrino searches and are summarized in TABLE II. The most general test is the one that we just described and that leads to the test statistic given in equation (9). We will indicate this test statistic with T_2 . This test is agnostic regarding the value of $\sin^2(2\theta)$ or Δm^2 and can be applied to search for a sterile neutrino with unknown parameters of interest.

The second test statistic used in the field can be traced back to the situation in which the mass squared difference is considered to be perfectly known and is equal to the value of the null hypothesis ($\Delta m^2 = Y$). In this case the alternative hypothesis and its related test statistic are:

$$H_1 : \{\sin^2(2\theta), \Delta m^2 : 0 \leq \sin^2(2\theta) \leq 1, \Delta m^2 = Y\} \quad (10)$$

$$T_1 = -2 \ln \frac{\sup_{\eta} \mathcal{L}(\sin^2(2\theta) = X, \Delta m^2 = Y, \eta | N^{obs})}{\sup_{\sin^2(2\theta), \eta} \mathcal{L}(\sin^2(2\theta), \Delta m^2 = Y, \eta | N^{obs})}. \quad (11)$$

While the numerator of T_1 is the same of T_2 , the maximum of the likelihood at the denominator is now computed over a narrower parameter space, restricted by the condition $\Delta m^2 = Y$.

The third test corresponds to the simplest kind of hypothesis test that can be performed. Both the null and alternative hypothesis have the parameters of interest fully defined. The alternative hypothesis is now the no-signal hypothesis and this leads to a test of the form:

$$H_1 : \{\sin^2(2\theta), \Delta m^2 : \sin^2(2\theta) = 0, \Delta m^2 = 0\} \quad (12)$$

$$T_0 = -2 \ln \frac{\sup_{\eta} \mathcal{L}(\sin^2(2\theta) = X, \Delta m^2 = Y, \eta | N^{obs})}{\sup_{\eta} \mathcal{L}(\sin^2(2\theta) = 0, \Delta m^2 = 0, \eta | N^{obs})}. \quad (13)$$

The numerator and denominator are the maximum likelihoods for fixed values of the parameters of interest, where the maximum is computed over the parameter space allowed for the nuisance parameters. The null hypothesis can now be rejected only if it is more unlikely than the alternative no-signal hypothesis. T_0 cannot be used to test the no-signal hypothesis otherwise the null and alternative hypothesis would be exactly the same.

TABLE II. Definition of the test statistics used for sterile-neutrino searches in the presence of nuisance parameters ($\boldsymbol{\eta}$). The null hypothesis is $H_0 : \{\sin^2(2\theta), \Delta m^2 : \sin^2(2\theta) = X, \Delta m^2 = Y\}$ for all tests while the alternative hypothesis H_1 changes. The dimensions of the parameter space associated to the test are shown in the second column. The name of the test statistics and of the techniques based on it are given in the third and fourth column. Examples of experiments using each test are given in the last column.

Test Statistic Computed for $H_0 : \{\sin^2(2\theta), \Delta m^2 : \sin^2(2\theta) = X, \Delta m^2 = Y\}$	Free Parameters of Interest	Test Statistic Name	Techniques Associated	Experiments
$T_2 = -2 \ln \frac{\sup_{\boldsymbol{\eta}} \mathcal{L}(\sin^2(2\theta) = X, \Delta m^2 = Y, \boldsymbol{\eta} N^{obs})}{\sup_{\sin^2(2\theta), \Delta m^2, \boldsymbol{\eta}} \mathcal{L}(\sin^2(2\theta), \Delta m^2, \boldsymbol{\eta} N^{obs})}$	$\sin^2(2\theta), \Delta m^2$	profile likelihood ratio	2D/global scan or global p-value	LSND, MiniBooNE, PROSPECT
$T_1 = -2 \ln \frac{\sup_{\boldsymbol{\eta}} \mathcal{L}(\sin^2(2\theta) = X, \Delta m^2 = Y, \boldsymbol{\eta} N^{obs})}{\sup_{\sin^2(2\theta), \boldsymbol{\eta}} \mathcal{L}(\sin^2(2\theta), \Delta m^2 = Y, \boldsymbol{\eta} N^{obs})}$	$\sin^2(2\theta)$	profile likelihood ratio	raster scan or local p-value	NEOS, STEREO
$T_0 = -2 \ln \frac{\sup_{\boldsymbol{\eta}} \mathcal{L}(\sin^2(2\theta) = X, \Delta m^2 = Y, \boldsymbol{\eta} N^{obs})}{\sup_{\boldsymbol{\eta}} \mathcal{L}(\sin^2(2\theta) = 0, \Delta m^2 = 0, \boldsymbol{\eta} N^{obs})}$	—	ratio of profile likelihoods	Gaussian CL _s	DANNS

Within the high-energy physics community, T_2 and T_1 are referred to as “profile likelihood ratio” test statistics whereas T_0 is sometimes called “ratio of profile likelihoods” [35, 36]. These names derive from the fact that the operation of maximizing the likelihood over the nuisance parameters is called profiling.

T_2 and T_1 can assume any positive real value. If the absolute maximum of the likelihood corresponds to H_0 , these test statistics are identically null. The farther the absolute maximum is from the parameter space of the null hypothesis, the larger the test statistic value becomes. According to Wilks’ theorem the probability distribution of these test statistics converges to a chi-square function in the large sample limit and when the null hypothesis is true, but only if a set of regularity conditions are met [37]. In particular, given the ratio between the dimensionality of the parameter space for the null and alternative hypothesis (i.e. the number of free parameters of interest in the likelihood maximization), T_2 would converge to a chi-square with two degrees of freedom and T_1 to a chi-square with one degree of freedom. As discussed in Section IV C, the conditions required by Wilks’ theorem are not always valid in sterile neutrino experiments and the assumption that the test statistic follows a chi-square distribution can lead to significantly inaccurate results.

The probability distribution of T_0 is qualitatively different from those of T_2 and T_1 . T_0 is negative when the maximum of the likelihood function in the parameter space of the null hypothesis is larger than in the space of the alternative (i.e. no-signal hypothesis), positive in the opposite case. Also in this case, the larger is the test statistic value, the stronger the null hypothesis is

disfavoured. The asymptotic properties of T_0 have been discussed in Ref. [10] according to which, under some mild conditions, the distribution of T_0 converges to a Gaussian distribution.

As previously mentioned, our results are based on test statistic probability distributions constructed from ensembles of pseudo-data. This procedure is discussed in detail in Appendix B. Firstly a grid in the $\sin^2(2\theta)$ vs. Δm^2 space is defined. Secondly, for each point on the grid an ensemble of pseudo-data is generated. The probability distributions are hence constructed by computing the test statistic for the pseudo-data in the ensemble. In our construction the nuisance parameters are kept fixed to a particular value. This approach is common with test statistics such as T_2 and T_1 whose probability distribution weakly depends on the true value of the nuisance parameters [11]. The value at which the nuisance parameters are fixed usually corresponds to the absolute maximum of the likelihood given the observed data set. To ease the comparison we use the same approach also for T_0 even if this test statistic does not automatically propagate the uncertainties due to the nuisance parameters through the analysis [35] and would require the construction of ensembles generated by sampling the nuisance parameters from some prior distribution [38].

The search for sterile neutrinos is generally performed without any limitation or preference on the value of $\sin^2(2\theta)$ or Δm^2 . All the parameter space accessible by the experiment is probed in search for a signal. This approach should naturally lead to analyses based on T_2 . The maximization of the likelihood required by T_2 is however challenging from the computational point of view. Reducing the dimensionality of the parameter

space over which the likelihood is maximized can enormously simplify the analysis and, for such a practical reason, many collaborations adopt T_1 or T_0 . In the neutrino community, the analysis based on T_2 has been called “2D scan” or “global scan” while the analysis based on T_1 is known as “raster scan” [8, 9]. In the absence of nuisance parameters, the definition of these test statistics reduce to those discussed in Ref. [8]. T_0 has been used in the framework of a method called “Gaussian CLs” [10].

The search for new particles at accelerators presents many similarities with the search for sterile neutrinos. For instance, in the search for the Higgs boson, the sought-after signal is a peak in an energy spectrum over some background. The two parameters of interest are the mass of the Higgs boson, which defines the energy of the peak, and its coupling with other particles, which defines the strength of the signal. Similarly, in the search for sterile neutrinos Δm^2 defines the shape of the signal and $\sin^2(2\theta)$ its strength. When the Higgs boson is searched without assumptions on its mass and coupling, a test similar to T_2 is performed (i.e. a “global p-value” analysis). When the mass is assumed to be known, a test similar to T_1 is used (i.e. a “local p-value” analysis) [39]. Procedures for converting a local into a global p-value have been developed in the last years [40, 41] and are nowadays used to avoid the direct usage of T_2 that is computationally demanding. This procedure is known as a correction for the “look-elsewhere effect”. We have tested this correction in the analysis of sterile neutrinos and found that it does not provide satisfactory results because of the oscillatory nature of the sought-after signature. Our studies on such a correction are discussed in Appendix E.

C. Signal Significance and p-values

The hypothesis testing discussed in the previous section is a procedure that defines when to accept H_0 or, alternatively, when to reject H_0 and accept H_1 . This procedure relies on whether the test statistic value computed for the observed data set is within the pre-defined critical region or not. The definition of the threshold – i.e. the definition of the size of the test – must be fixed prior the experiment in order to avoid biases. However, in addition to the dichotomous decision on the acceptance/rejection of H_0 , it can be useful to report how far the observed value of the test statistic is from the edge of the critical region. This can be given using the “p-value” that is equivalent to the minimal test size that is needed to reject the null hypothesis. For instance, if the p-value for an observed data set is 4%, it means that the null hypothesis would be rejected by a test with $\alpha = 5\%$, but not by a test with $\alpha = 3\%$. A more formal definition of the p-value can be found in Appendix C.

When searching for a new physics phenomenon, testing the hypothesis that there is no signal is of primary interest as a discovery is claimed when the no-signal hy-

pothesis is rejected. In the search for sterile neutrinos the no-signal hypothesis corresponds to $H_0 : \{\sin^2(2\theta), \Delta m^2 : \sin^2(2\theta) = 0 \text{ or } \Delta m^2 = 0\}$. Indeed, according to equations (1) and (2), there is no oscillation if at least one of the two parameters of interest is null. This detail is important because the no-signal hypothesis is always part of H_1 even when the test is based on T_1 and the value of Δm^2 is fixed.

In the following we will refer to the significance of a discovery as the p-value under the no-signal hypothesis. This is computed by performing a hypothesis test in which H_0 is any of the parameter combinations corresponding to absence of the signal that are included in the space of the alternative hypothesis.

D. Interval Estimation and Confidence Regions

The primary way to display the result of a neutrino oscillation search is a two-dimensional confidence region in the $\sin^2(2\theta)$ vs. Δm^2 space. The confidence region is a set of parameters values that are compatible with the data given a certain confidence level. The construction of a confidence region is formally referred to as an interval estimation.

One of the most popular statistical techniques to construct a confidence region is through the inversion of a set of hypothesis tests [34, 42]. This is also the technique used by experiments searching for sterile neutrinos. The construction starts from the selection of a specific test and its resulting test statistic. The parameter space considered for H_1 is naturally the space in which the region will be defined. Usually a grid is fixed over this space and a test is run for each point. The tests in this set have the same H_1 but H_0 is changed to the value of the parameters at each point. This canonical construction guarantees that the properties of the test statistic carry over to the confidence region. For instance, unbiased tests, when inverted, will produce unbiased confidence regions. The confidence level is also preserved and a 95% C.L. test leads to a 95% C.L. confidence region. In addition, since likelihood ratio test statistics are among the most powerful test in many applications, their inversion provides regions with close to minimal size. Constructing regions with minimal size is clearly an advantage as the results of an experiment will define a narrower allowed range for the parameter values.

Since the confidence region is constructed in the parameter space considered by the alternative hypothesis, tests based on T_2 would naturally lead to two-dimensional confidence regions in the $\sin^2(2\theta)$ vs. Δm^2 space, tests based on T_1 to one-dimensional regions in the $\sin^2(2\theta)$ space, and tests based on T_0 to point-like regions. As we already mentioned, T_0 and T_1 are often used improperly in the sense that the experimenter does not want to restrict the parameter space but just to simplify the analysis. In this case, two-dimensional confidence regions can be constructed as union of one-

dimensional or point-like regions. For instance, while T_1 would require the value of Δm^2 to be known, one could technically construct a one-dimensional $\sin^2(2\theta)$ region for a scan of “known” Δm^2 values and then take the union of this regions. Assuming that the true Δm^2 is among the scanned values, the confidence level of the union will be the same of the test. Two-dimensional confidence regions obtained from this non-canonical procedure can however have unexpected properties and pathological behaviours. In particular, the size of the region can become increasingly large with the number of Δm^2 values scanned. Similar considerations apply to T_0 for which a scan over “known” values of Δm^2 and $\sin^2(2\theta)$ is needed.

E. Sensitivity

The comparison of the different kind of hypothesis testing discussed in Section III B will be based on the confidence region constructed for some reference data sets of our toy experiments. In addition, we will extensively use the concept of sensitivity for limit setting and signal discovery. Both sensitivities will be displayed as contours in the $\sin^2(2\theta)$ vs. Δm^2 parameter space. The contour of the sensitivity for limit setting connects the hypothesis for which we would expect a median p-value of 5% if the no-signal hypothesis were true. Instead, the contour of the sensitivity for signal discovery connects the hypothesis that if were true, would give a median significance of 5%. A discovery is usually associated to a smaller median significance (e.g. a p-value=0.027 or even $6 \cdot 10^{-7}$) but we prefer to compare the sensitivity for limit setting and signal discovery for the same significance in order to emphasize their differences.

The sensitivity for limit setting is conceptually equivalent to the edge of the confidence region that we would expect to measure if there were no signal. The sensitivity for signal discovery is instead the edge of the parameter space for which we expect to be able to reject the no-signal hypothesis and thus make a discovery. Basically, it is the parameter space in which the test is able to discriminate between the signal and no-signal hypothesis. More details on how the sensitivities are defined and computed are provided in Appendix C.

IV. TEST BASED ON PROFILE LIKELIHOOD RATIOS

In this section we compare the results of hypothesis tests based on the two profile-likelihood-ratio test statistics, i.e. T_2 and T_1 . The comparison is done using the toy experiments introduced in Section II: a disappearance experiment representative of searches based on reactor neutrinos and an appearance experiment representative of the accelerator-based experiments. First we focus on the sensitivity of the toy experiments (Sec-

tion IV A) and then consider the results extracted for specific sets of data (Section IV B). Finally, in Section IV C, we study the impact of approximating the test statistic distributions with chi-square functions.

A. Sensitivity

The sensitivity for limit setting and signal discovery of our toy disappearance experiment based on the statistic T_2 is shown in FIG. 2a. The sensitivity for limit setting (black lines) delimits the parameter space that is expected to be rejected by a 95%-C.L. test with 50% probability under the assumption that sterile neutrinos do not exist. The sensitivity for signal discovery (red lines) delimits the set of hypotheses assuming which a signal would be observed in 50% of the cases and the no-signal hypothesis rejected by a 95%-C.L. test. The figure shows separately the sensitivity for a rate and shape analysis (dotted lines). The total sensitivity (continuous line) is not the linear combination of the two contributions. Nevertheless it is useful to display them in order to understand which kind of information contributes most to the sensitivity at a given Δm^2 value. Three Δm^2 regions can be identified in FIG. 2a:

- $\Delta m^2 > 10 \text{ eV}^2$: the oscillation length is smaller than the detector resolution on L_{rec} and/or E_{rec} , making the experiment sensitive only to an overall reduction of the integral rate (sensitivity dominated by the rate analysis);
- $0.1 < \Delta m^2 < 10 \text{ eV}^2$: the oscillation length is larger than the experimental resolution and smaller than the range of L_{rec} and/or E_{rec} values accessible by the detector, making the experimental sensitivity dominated by the shape analysis;
- $\Delta m^2 < 0.1 \text{ eV}^2$: the integral rate is no more affected by sterile neutrinos and the oscillation length becomes larger than the detector dimensions, resulting in a loss of sensitivity for both the rate and shape analysis.

Example of the expected oscillations in these three regions are shown in FIG. 1b and 1c.

As already mentioned, the total sensitivity is not given by the sum of the sensitivity of the rate and shape analysis. The rate and shape analysis are indeed emulated by considering only parts of the likelihood function (see Section III A) that otherwise share parameters and have a non trivial interplay. For instance, the sensitivity for the rate analysis is even higher than the total one for high Δm^2 values. This feature is related to the fact that $\sin^2(2\theta)$ and Δm^2 are fully degenerate parameters in a rate analysis based on T_2 . Given an observed number of events, the global maximum of the likelihood function can be obtained for infinite combinations of $\sin^2(2\theta)$ and Δm^2 values. The degeneracy is however broken when the rate information is combined with the shape one. The

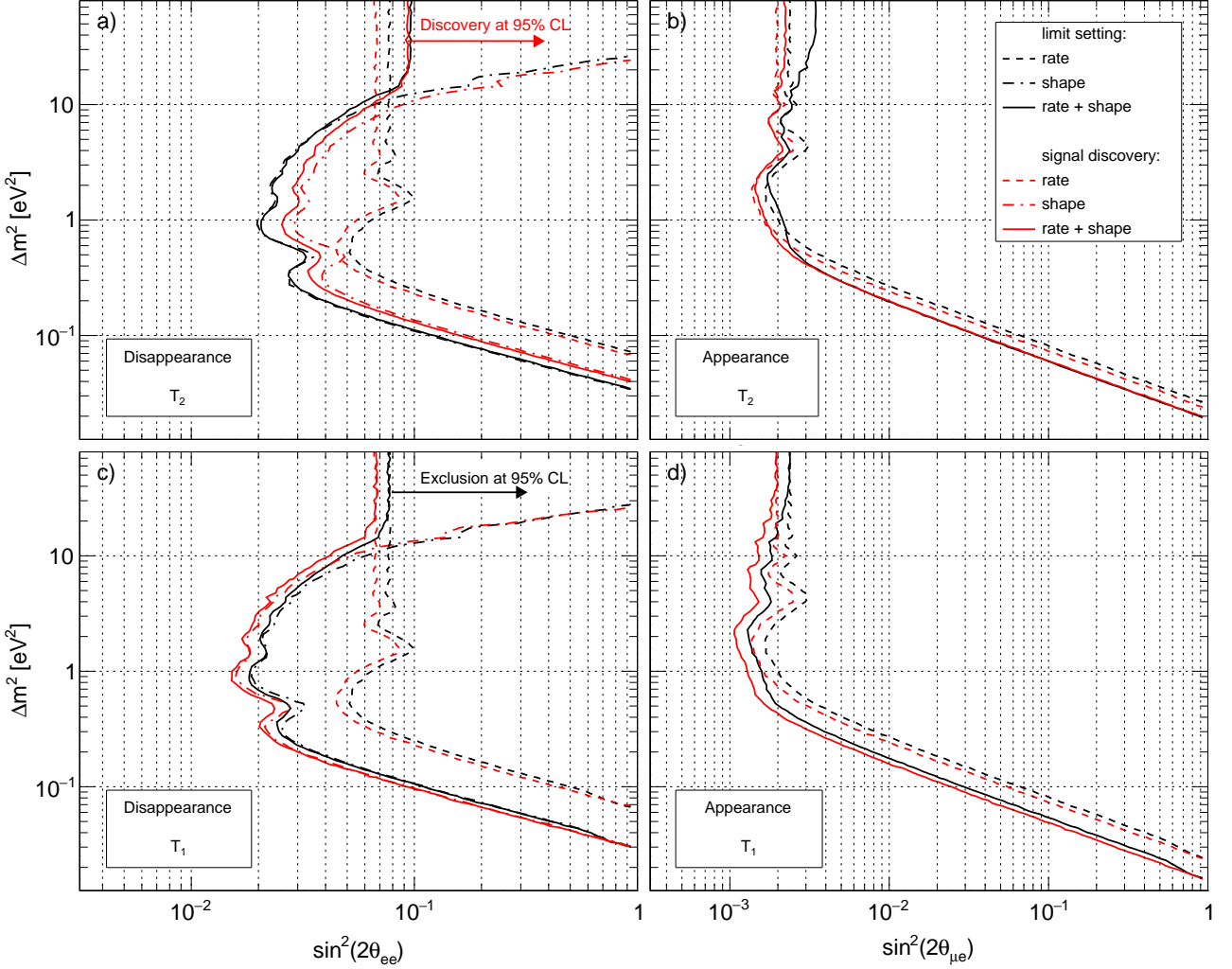


FIG. 2. Sensitivity for limit setting and signal discovery at 95% C.L. for a toy disappearance and appearance experiment. The sensitivities are shown for the test statistics T_2 and T_1 . Whenever possible, the contribution of the shape and rate analysis are displayed separately.

number of effective degrees of freedom of the problem changes, and this results in a reduction of sensitivity.

The sensitivities of our toy appearance experiment computed for T_2 is shown in FIG. 2b. The same Δm^2 regions discussed for the disappearance experiment can be identified, even if the relative weight of the shape and rate information is different. In particular, in the appearance searches a shape analysis can provide information on Δm^2 but not on $\sin^2(2\theta)$. The number of expected ν_e events is indeed proportional to the product of the oscillation amplitude $\sin^2(2\theta)$ and flux of ν_μ neutrinos. If the flux is left unconstrained in the fit, no statement can thus be made about the oscillation amplitude. This is the reason why the shape analysis contribution is not separately displayed. The rate analysis accounts for the bulk of the sensitivity and adding the shape information does not result in a net improvement, in the sense that the slight improvement is compensated by the reduction

of sensitivity due to the increased number of effective degrees of freedom discussed above. Having a sensitivity dominated by the rate analysis is typical for experiments using accelerators as neutrino source.

The sensitivity for limit setting and signal discovery are similar between each other for both the disappearance and appearance experiment. Some differences are however present. When computing the sensitivity for signal discovery, the hypothesis tested is the no-signal hypothesis. Since $\sin^2(2\theta) = 0$ or $\Delta m^2 = 0$ are points at the edge of the allowed parameter space, the number of degrees of freedom of the problem decreases when testing them and the power of the test increases. The sensitivity for limit setting is instead computed for values of the parameters far from the edges. This is the reason why the sensitivity for signal discovery is in general expected to be stronger than that for limit setting. However the situation is reversed in the shape analysis because of a pe-

cular feature of the sterile neutrino signature. Statistical fluctuations between bins mimic an oscillation signal and the maximum of the likelihood is always found far from the no-signal hypothesis. This decreases significantly the power of the test for signal discovery while it does not affect much the sensitivity for limit setting. If the shape analysis dominates the overall sensitivity, as in our disappearance experiment, its features propagate also to the combined sensitivities.

FIG. 2c and 2d show the sensitivities for our toy disappearance and appearance experiments computed for T_1 . The overall features are similar to those of T_2 and the weight of the rate and shape information in the three Δm^2 regions are also consistent. However, since the parameter space of the alternative hypothesis is now restricted, T_1 leads to sensitivities that are up to 45% stronger in terms of $\sin^2(2\theta)$. This is particular evident for high Δm^2 values where, differently from T_2 , now the number of effective degrees of freedom in the alternative hypothesis is always one (only $\sin^2(2\theta)$ is free) and the total sensitivity is equal to the one from the rate analysis. The restriction of the parameter space is also the reason why the maximum of the likelihood can now correspond to the no-signal hypothesis and the sensitivity for signal discovery is stronger than that for limit setting even in a shape analysis.

It should be emphasized that the mixing angle in the plot for the disappearance experiment is different from that of the appearance experiment. The minimal value of $\sin^2(2\theta)$ accessible by an experiment cannot be used as a figure of merit to compare disappearance and appearance experiments. A comparison can however be done assuming a specific theoretical model that connects the value of $\sin^2(2\theta_{ee})$ and $\sin^2(2\theta_{\mu e})$ [7].

B. Results from Observed Data Sets

The confidence region derived from an observed data set can significantly differ from the expectations because of statistical fluctuations on the number of signal and background events. This issue is particularly relevant when no signal is observed and an upper limit on a parameter is reported. The upper limit can indeed exceed the sensitivity of the experiment by orders of magnitude.

In sterile neutrino searches, when no signal is observed, the confidence region extends down to $\sin^2(2\theta) = 0$ for most of the Δm^2 values and it is bounded by an upper limit on $\sin^2(2\theta)$ that plays the role of the maximum signal strength. It is hence informative to report the observed upper limit along with its expected value and variance under the no-signal hypothesis. This has been first proposed in Ref. [8] and it is nowadays a standard in particle physics.

FIG. 3a shows the confidence region derived with T_2 from a pseudo-data set generated for the toy disappearance experiment under the no-signal hypothesis. In addition to the confidence region, the expected distribution of

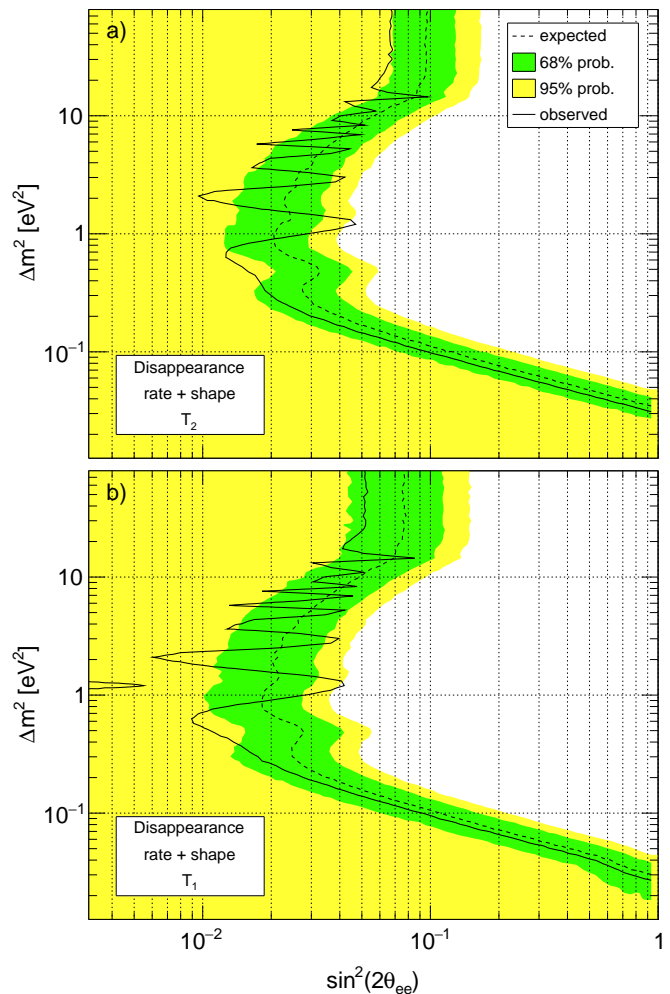


FIG. 3. Confidence regions at 95%-C.L. for a pseudo-data set generated by the toy disappearance experiment under the no-signal hypothesis. The top plot is obtained using T_2 while the bottom plot using T_1 . The probability distribution of the upper bound of the confidence region expected under the no-signal hypothesis is displayed through its median value (i.e. the sensitivity for limit setting) and the 68% and 95% central intervals.

the upper limit is displayed in terms of its median value and 68%/95% central intervals. The median is exactly the sensitivity for limit setting plotted in FIG. 2a. The observed upper limit fluctuates around the median expectation. This is true for all possible realizations of the data as the likelihood is maximized for a specific phase of the oscillatory pattern that matches the statistical fluctuations between the bins of the data set. This phase is reproduced at regularly spaced values of Δm^2 over the full parameter space. The limit gets weaker when the phase helps describing the data, stronger when it does not. The overall shift of the observed limit with respect to the median value is instead due to the fact that the random number of events injected in the data set is slightly above its median expectation. The width of the

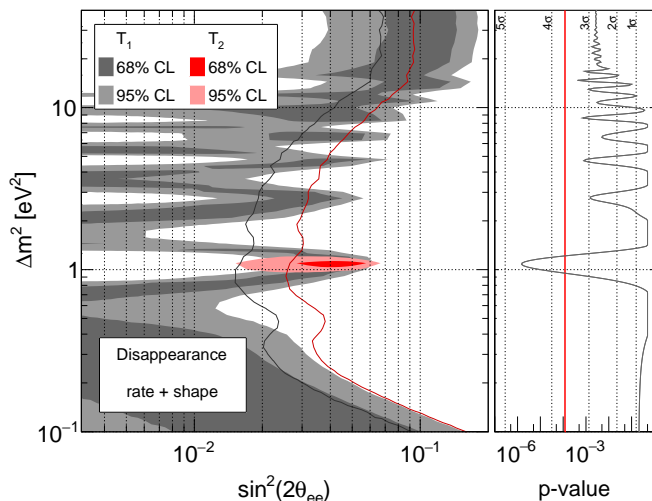


FIG. 4. Confidence regions at 68% and 95% C.L. for pseudo-data generated by the toy disappearance experiment assuming the existence of a sterile neutrino with $\sin^2(2\theta) = 0.04$ and $\Delta m^2 = 1 \text{ eV}^2$. The 95% C.L. sensitivity for signal discovery is shown for both the statistic T_2 (red line) and T_1 (grey line). The p-values for the no-signal hypothesis (i.e. the significance of a signal) are shown in the right panel: T_2 provides a unique p-value (red line) whereas T_1 provides a p-value for each Δm^2 value tested (grey line).

green and yellow bands gives an idea of the magnitude of the fluctuations as they contain the upper limit with a probability of 68% and 95% respectively.

The results and expectations based on T_1 are shown in FIG. 3b. We remind the reader that the two-dimensional confidence regions constructed with T_1 can be considered as the union of one-dimensional confidence regions in the $\sin^2(2\theta)$ space, each computed for a fixed Δm^2 value that is considered to be known. The analysis based on T_1 exhibits features similar to what obtained for T_2 . The fluctuations of the upper limit around its median expectation are now slightly stronger as the tests performed at different Δm^2 values are independent from each other. The magnitude of the fluctuations is quantified by the width of the 68% probability central interval. An other important difference between the two statistics is that while T_2 can either reject or accept the no-signal hypothesis (i.e. all the hypotheses with $\sin^2(2\theta) = 0$), T_1 can accept it at some Δm^2 value and reject it at other values. The figure shows for instance a range of Δm^2 values around 1 eV^2 in which the no-signal hypothesis is rejected.

The difference between the outcome of a test based on T_2 and one based on T_1 is much larger when a signal is present in the data. FIG. 4 shows the set of hypotheses accepted by the two tests for a pseudo-data set generated assuming a sterile neutrino with $\sin^2(2\theta) = 0.04$ and $\Delta m^2 = 1 \text{ eV}^2$. For each test, the confidence regions at 68% and 95% C.L. are shown along with the sensitivity for signal discovery. The analyses based on T_2 is able to properly pin down the signal and it returns a

two-dimensional confidence region surrounding the true parameter values. On the other hand, T_1 yields a one-dimensional $\sin^2(2\theta)$ confidence region for each Δm^2 . For Δm^2 values close to the true one, T_1 returns a region that is similar to that of T_2 . However, for most of the other Δm^2 values it also returns a region that does not contain the no-signal hypothesis. The non-standard construction of the confidence region results in regions that do not constrain the parameter Δm^2 , coherently with the fact that this parameter is supposed to be known in T_1 .

The significance of the signal is shown on the right panel in terms of the p-value for the no-signal hypothesis as defined in Section III C. The significance for a test based on T_2 is 10^{-4} (equivalent to a 3σ two-sided Gaussian deviation). The p-value computed for T_1 depends on the assumed Δm^2 value and reaches a minimum value of 10^{-6} around the Δm^2 corresponding to the injected signal (equivalent to a 4σ two-sided Gaussian deviation). As expected the significance obtained with T_1 is stronger. If the Δm^2 value is actually unknown, the results of T_1 are overestimated because of the look-elsewhere effect.

C. Validity of Wilks' theorem

Constructing the probability distributions of the test statistic through Monte Carlo methods can be computationally challenging and often it is avoided by invoking the asymptotic properties of the generalized likelihood ratio test. If the regularity conditions required by Wilks' theorem are met [37], T_2 and T_1 are indeed expected to follow a chi-square distribution with a number of degrees of freedom equal to the effective number of free parameters of interest [36]. One requirement of Wilks' theorem is that the maximum likelihood estimators converge to a normal distribution around its true value. Sterile neutrino experiments do not typically fulfill this condition as $\sin^2(2\theta)$ is reconstructed next to the border of its allowed range (only positive values are physically allowed) or far from its true value when the statistical fluctuations mimic a fake signal.

The applicability of Wilks' theorem is here studied through the concept of coverage probability, i.e. the probability that the confidence region covers the true value of the parameters of interest. If the test statistic probability distribution is perfectly known and independent of the nuisance parameters, the coverage is equal to the confidence level of the test used to construct the confidence region. If the probability distribution is approximated by a chi-square function, the coverage can in principle vary significantly from the confidence level of the test. Overcoverage refers to situations in which the coverage is larger than the confidence level of the test, undercoverage if it is smaller. The coverage is computed by generating an ensemble of pseudo data for a given hypothesis and counting what is the fraction of times that the reconstructed confidence region includes it. The operation is repeated for many different hypothesis in order

to map it as a function of $\sin^2(2\theta)$ and Δm^2 parameters.

The coverage probability computed for T_2 assuming the validity of Wilks' theorem is shown in FIG. 5 for both our toy disappearance and appearance experiments and considering separately a rate and shape analysis. The test statistic distributions have been approximated by a chi-square with one or two degrees of freedom, according to the number of non-degenerate parameters of interest in the alternative hypothesis (see insets in the figure).

The coverage is generally correct in the parameter space where the experiment is sensitive to a signal. The rate analysis shows just a slight overcoverage where the experiment is not sensitive. This is expected as $\sin^2(2\theta)$ is bounded to positive values, causing an effective reduction of the degrees of freedom of the test when the signal is reconstructed close to the edge of the allowed parameter space [43].

The shape analysis has instead a severe undercoverage for $\sin^2(2\theta)$ values below the sensitivity of the experiment and the coverage can be as low as 60%. The undercoverage is connected to the fact that when a binned analysis is performed, it is always possible to find a sterile neutrino hypothesis whose oscillatory pattern helps reproducing the statistical fluctuations between bins. As a result, even if no signal is present in the data, the maximum of the likelihood always corresponds to some oscillation hypothesis. This is conceptually equivalent to overfitting and it artificially increases the degrees of freedom of the test and the test statistic values (see discussion in Appendix D). A region of overcoverage is present also in the parameter space within the sensitivity of the experiment at low Δm^2 values, where the oscillation length becomes close to the dimension of the detector, creating a degeneracy between the parameters of interest. Together with the restriction of the parameter space ($\sin^2(2\theta) \leq 1$), the number of effective degrees of freedom changes.

When the analysis includes both the rate and shape information, the coverage shows a combination of the features discussed above. In particular, in the parameter space beyond the sensitivity of the experiment, the overcoverage of the rate analysis partially compensates for the undercoverage of the shape analysis. Severe undercoverage regions are however still present, consistently with the results obtained in Ref. [8].

The difference between the outcome of a test based on probability distributions constructed with Monte Carlo techniques and their chi-square approximation is shown in FIG. 6. Both the sensitivities and the confidence regions reconstructed from pseudo data are significantly different, up to 70% in terms of $\sin^2(2\theta)$. For experiments with a sensitivity dominated by the shape analysis, the confidence region can even switch from an upper limit to an island, leading to a unjustified claim for a signal. The probability for this event to occur can be significant, up to 40% in our toy experiment for the considered hypothesis.

While the asymptotic approximation is not satisfactory for tests based on T_2 , it is instead very good for

tests based on T_1 . The coverage of T_1 has exactly the same features of FIG. 5a and 5d and it is not shown here. The coverage is correct in the region to which the experiment is sensitive and is slightly higher (97.5%) in the parameter space beyond the experimental sensitivity. The possibility of avoiding a Monte Carlo construction of the probability distributions of T_1 is a significant advantage and contributed to make T_1 popular in the sterile neutrino community.

V. TEST BASED ON RATIO OF PROFILE LIKELIHOODS

The sensitivity for limit setting based on T_0 for our toy disappearance experiment is shown the first row of FIG. 6 separately for the rate, shape and combined analysis. This test provides a sensitivity significantly stronger than what obtained with T_2 and T_1 . This is coherent with the fact that the parameter space for the alternative hypothesis is now extremely restricted and the power of the test is close to maximum. The sensitivity for signal discovery cannot be calculated for T_0 because, as explained in Section III B, this test cannot be used to evaluate the no-signal hypothesis.

The confidence regions extracted for a specific pseudo-data sets not containing a signal is shown in the second row of FIG. 6. T_0 can set extremely stringent constraints on $\sin^2(2\theta)$ that are orders of magnitudes beyond the sensitivity. This is again related to the very limited parameter space available for the alternative hypothesis. Since the test has almost no degrees of freedom, a small preference for the no-signal hypothesis can be enough to reject the null hypothesis. To mitigate this behaviour this test statistic has been used only in combination with the CL_s method [44] that penalizes constraints stronger than the sensitivity by introducing an overcoverage in the test. The combination of T_0 and the CL_s method is known as "Gaussian CL_s " [10].

The plots in the fourth row of FIG. 6 show the confidence regions extracted for a pseudo-data set containing a signal. Because of the non-standard construction of the two-dimensional confidence region, neither the value of Δm^2 or $\sin^2(2\theta)$ are properly constrained by T_0 . Indeed for any given Δm^2 value, it will always be possible to find a $\sin^2(2\theta)$ value that is accepted by the test and, viceversa, for any given $\sin^2(2\theta)$ it will always be possible to find a Δm^2 value that is accepted. This test is hence not suitable to handle a data set with a signal.

We confirmed that the probability distribution of T_0 converges to a normal distribution for our toy appearance and disappearance experiment as reported by Ref. [10] to which we refer the reader for further information.

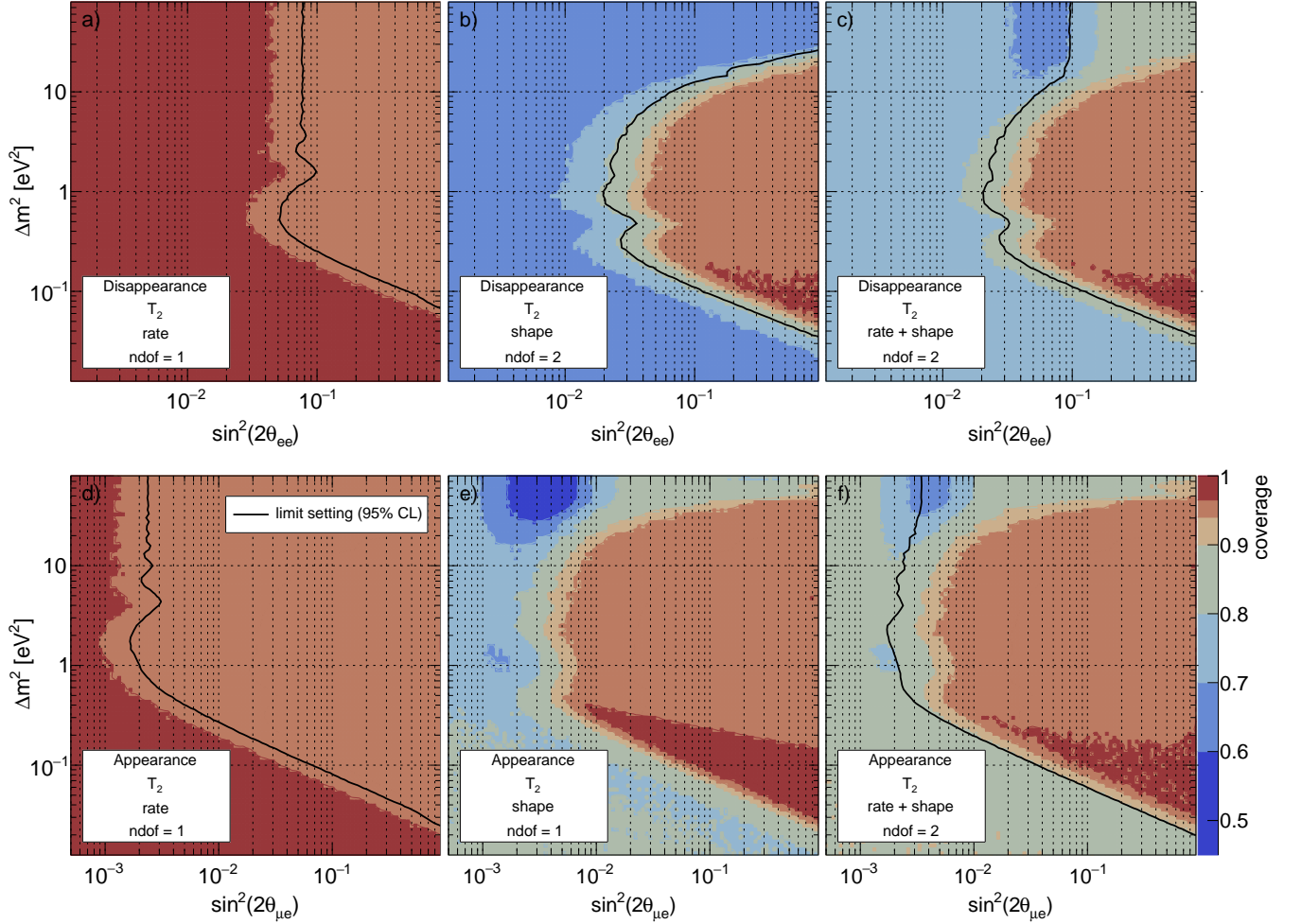


FIG. 5. Coverage of the 95%-C.L. confidence region based the test performed with T_2 and assuming that this test statistic follows chi-square distributions. The number of degrees of freedom of the chi-square distribution is chosen according to the number of non-degenerate parameters in the likelihood. The top panels show the coverage probability for the toy disappearance experiment, the bottom panels for the toy appearance experiment. For each kind of experiment the coverage for a rate analysis (left), a shape analysis (middle) and the full analysis (right panel) are shown separately. The color palette used to show the coverage probability is the same in all plots. The 95% C.L. sensitivity for limit setting is also displayed to delimit the parameter space in which the experiment is sensitive.

VI. COMPARISON AND DISCUSSION

The main difference among the statistical methods applied to the search for sterile neutrinos has been traced back to the definition of the alternative hypothesis in the hypothesis testing procedure. The considered definitions lead to three different test statistics whose properties are summarized in the following.

The parameter space considered in a test based on T_2 includes all possible values of $\sin^2(2\theta)$ and Δm^2 . Using this test for an interval estimation procedure provides naturally two-dimensional confidence regions (in the $\sin^2(2\theta)$ vs. Δm^2 space) that are expected to have close-to-minimal size. Adopting this test statistic is appropriate when the value of the parameters of interest is unknown and a generic search over the full parameter

space is intended. The statistic T_2 can be used to estimate the significance of a potential signal by performing a test of the no-signal hypothesis. The probability distributions of this test statistic are not well approximated by chi-square functions in the analysis of sterile neutrino experiments, and such an approximation can lead to very inaccurate confidence regions and even to erroneously rejecting the no-signal hypothesis.

A test based on T_1 is appropriate when the value of Δm^2 is assumed to be known prior to the experiment. In this condition the test can be used to construct a one-dimensional confidence region in the $\sin^2(2\theta)$ space and estimate the significance of a signal by testing the no-signal hypothesis ($\sin^2(2\theta) = 0$). If this test is improperly used to search for a signal at different Δm^2 , the union of $\sin^2(2\theta)$ confidence regions can be considered as

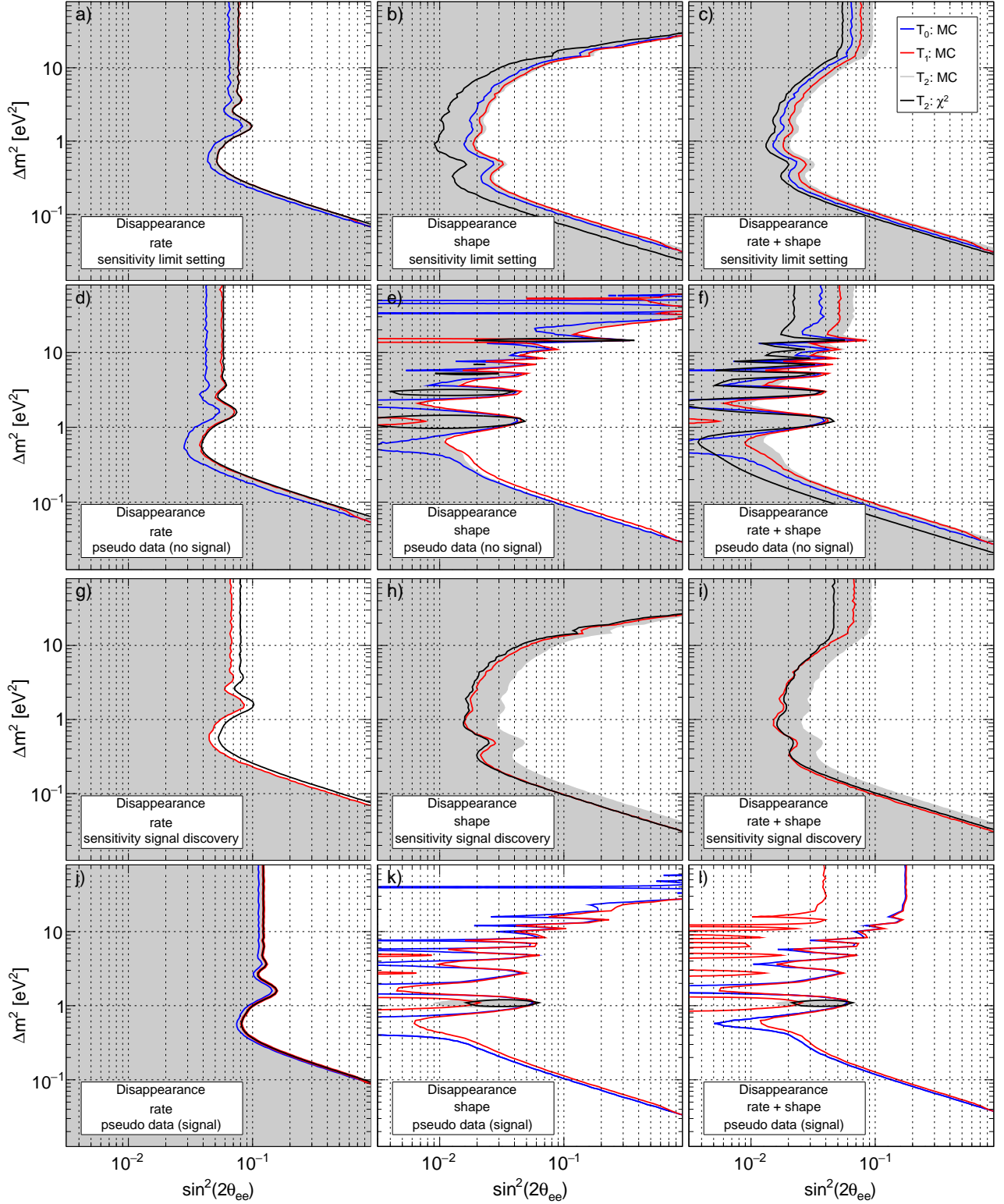


FIG. 6. Comparison of the sensitivity and confidence regions for the toy disappearance experiment obtained with T_2 , T_1 and T_0 . The figure shows: the sensitivity for limit setting (first row), the confidence regions for a pseudo-data set generated under the no-signal hypothesis (second row), the sensitivity for signal discovery (third row), and the confidence regions for a pseudo-data set generated assuming a sterile neutrino signal with $\sin^2(2\theta)=0.04$ and $\Delta m^2=1 \text{ eV}^2$ (fourth row). The rate (left) and shape analysis (middle) are shown independently and combined together (right column). The probability distribution of the test statistics are computed using Monte Carlo techniques. Results obtained when approximating the distributions with chi-square functions are shown for T_2 .

a two-dimensional confidence region but its size can be very far from optimal. Indeed, in case of a signal, the no-signal hypothesis can be rejected by tests performed for most of the Δm^2 values, making unclear where the actual signal is. If the significance of a signal is then taken as the stronger one among the tests performed, its value will be overestimated because of the look-elsewhere effect. Corrections for the look-elsewhere effect are currently not available for short-baseline experiments. The conditions for Wilks' theorem are found to be fulfilled by this test statistic and its probability distribution follows accurately a chi-square function.

The test statistic T_0 compares two simple hypotheses with a fixed value of the parameters of interest. The alternative hypothesis is defined as the no-signal hypothesis. Thus, the no-signal hypothesis can not be tested and the significance of a signal can not be computed. Furthermore, the test can only reject hypotheses more unlikely than the no-signal hypothesis resulting in confidence regions always connected to the no-signal hypothesis. The natural confidence regions constructed using this test are point-like. Two-dimensional regions in the $\sin^2(2\theta)$ vs Δm^2 can be obtained as union of many point-like confidence region. This lead to some pathological behaviour such as that neither the value of $\sin^2(2\theta)$ or Δm^2 can be narrowed in case of a signal. The probability distribution of this test statistic seems to follow their asymptotic functions but a Monte Carlo construction is probably anyway needed to properly account for the systematic uncertainties.

Regardless of the context in which each test should naturally be used, we compare in FIG. 6 the performance of the three test statistics for a generic search of sterile neutrinos with unspecified $\sin^2(2\theta)$ and Δm^2 values. Such a comparison can be used to evaluate how inaccurate are the results obtained with T_0 and T_1 . The sensitivity for limit setting and signal discovery computed with T_1 and T_0 is overestimated up to 20-30% in terms of $\sin^2(2\theta)$ values. The overestimation is related to the look-elsewhere effect. The statistic T_0 gives better sensitivity than T_1 , that in turn gives better sensitivity than T_2 . This should of course be considered when comparing experiments that use different test statistics.

The actual contours in the $\sin^2(2\theta)$ vs. Δm^2 space derived for a specific data set can also be extremely different. If no signal is observed (second row in FIG. 6), T_0 and T_1 can reject hypotheses with $\sin^2(2\theta)$ values orders of magnitude above the sensitivity. This is not the case for T_2 . The differences are even larger when a signal is present in the data (fourth row in FIG. 6). In this case T_2 pins down the true hypothesis, whereas the other methods accept hypotheses at any Δm^2 value and, in case of T_0 , also for a large range of $\sin^2(2\theta)$ values. This kind of differences are expected for most of the experiments as they affect both the rate analysis, the shape analysis, and their combination.

To easy the comparison of the performance and results from different experiments, it would be convenient for the

field to adopt a standardized analysis procedure. Based on the results presented in this article, such a standard analysis could follow these steps:

1. identification of the most likely value for $\sin^2(2\theta)$ and Δm^2 defined as the value corresponding the maximum of the likelihood function over the space $\{\sin^2(2\theta), \Delta m^2 : 0 \leq \sin^2(2\theta) \leq 1, \Delta m^2 \geq 0\}$ (i.e. maximum likelihood estimators);
2. check that the model corresponding to the most likely value of the parameters of interest is compatible with the data by using a "likelihood ratio" goodness-of-fit test [11] whose probability distribution is verified or constructed with Monte Carlo techniques¹;
3. test the no-signal hypothesis using the test statistic T_2 and report its significance;
4. construct the two-dimensional confidence region based on T_2 and report it including the sensitivity.

If the no-signal hypothesis is accepted by the test at point 3, the confidence region will extend down to vanishing $\sin^2(2\theta)$ values and its upper limit can be plotted along with its median value and 68/95% central intervals expected under the no-signal hypothesis (as in FIG. 3). If the no-signal hypothesis is instead rejected, the confidence region can be plotted for different confidence levels along with the sensitivity for signal discovery as in FIG. 4. The procedure proposed here is consistent and extends what has been recommended in Ref. [8].

When the number of events observed by an experiment is large and each bin of the data set contains tens of counts or more, the Poisson probability in the likelihood function can be approximated by a Gaussian probability. In this case, the likelihood function can be converted into a chi-square function. This treatment can be regarded as a sub-case of what is discussed in the previous sections. However, independently by the number of events, Wilks' theorem is not valid for T_2 because of the presence of physical borders and of the oscillatory nature of the sought-after signal. The construction of the test statistic probability distribution through Monte Carlo techniques is hence mandatory in order to ensure accurate results. The Monte Carlo construction is computationally demanding, but it is feasible as proved by the experiments that are already performing it. Indeed, the proposed analysis procedure is very similar to the what is used by e.g. MiniBooNE and PROSPECT.

¹ We studied the probability distribution of the likelihood-ratio goodness-of-fit test for a large number of configurations of our disappearance experiment and found that generally it can be approximated with a chi-square function. Nevertheless, we also identified some situations, e.g. in a shape analysis, in which the distribution follows a chi-square function with a number of degrees of freedom different from the expected one.

VII. CONCLUSIONS

The statistical methods used to search for short-baseline neutrino oscillations induced by an hypothetical sterile neutrino with mass at the eV scale have been reviewed and compared. Three hypothesis testing procedures are used in the field, each corresponding to a specific test statistic. Two out of the three test statistics make assumptions on the value of the parameters of interest for sterile neutrinos, i.e. Δm^2 and/or $\sin^2(2\theta)$. They hence do not reflect the question of interest for an experimenter who is searching for a generic sterile neutrino with unknown $\sin^2(2\theta)$ and Δm^2 values. The usage of these tests is possibly related to the computational difficulty of considering the general case with unknown parameters.

The impact of using the different test statistics has been explored under limit setting and signal discovery scenarios for a comprehensive set of experimental conditions. In particular, a toy appearance and a toy disappearance experiment have been used as test bench, considering for each the case in which the sensitivity is dominated by the information on the rate, on the shape or by their combination. The performance of the methods are studied in terms of the median constraints on the oscillation parameters estimated from ensembles of pseudo-data (i.e. the sensitivity) and for single data sets. The overestimation of the results obtained with test statistics that fold into the analysis prior assumptions on the value of the parameters of interest is found to be significant. The usage of different methods prevents a direct comparison of the results of different experiments and is not beneficial for the field. We thus propose a standard analysis based on the most general test statistic and the construction of its probability distribution through Monte Carlo techniques.

ACKNOWLEDGMENTS

The authors are greatly thankful to Hans Niederhausen for the valuable suggestions on how to interpret the statistical methods and structure the comparison. The authors would also like to thank T. Lasserre, P. Litchfield, L. Oberauer, G. Ranucci, M. Wurm and S. Schoenert for many helpful discussions and suggestions during the work and the preparation of the manuscript. This work has been supported by the Deutsche Forschungsgemeinschaft (SFB1258).

Appendix A: The Likelihood and Its Maximization

The general form of the likelihood used in the analysis of sterile neutrino experiments is given in Section III A. The computational task of finding the maximum of the likelihood is typically performed by minimizing the negative logarithm of the likelihood (NLL). Moving to the log-

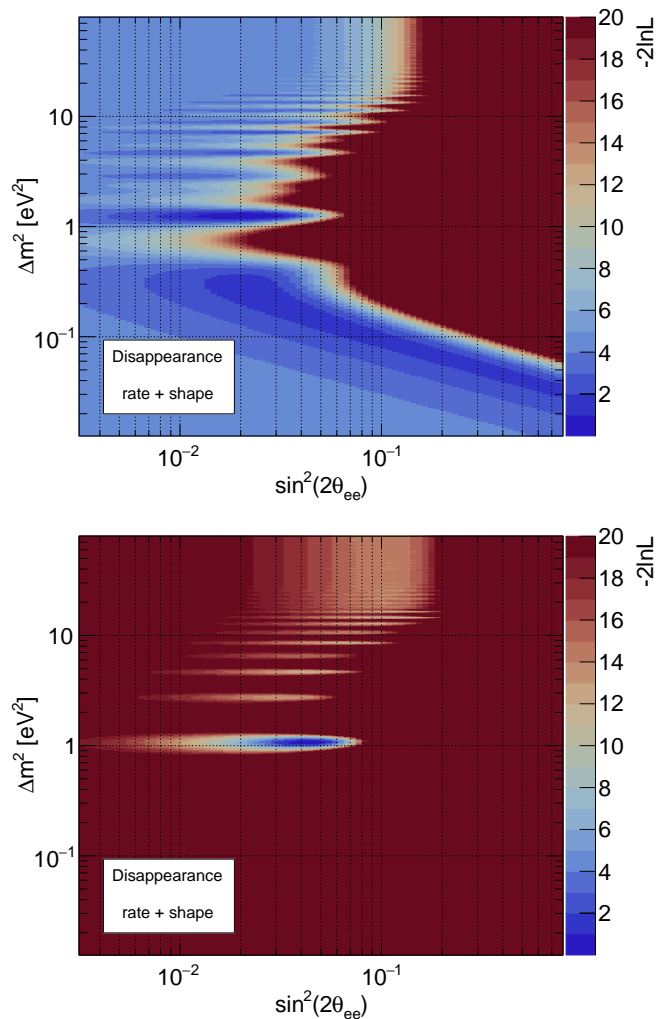


FIG. 7. Negative logarithm of the likelihood function for two sets of pseudo-data generated for the toy disappearance experiment, assuming the no-signal hypothesis (above) and the existence of a sterile neutrino with $\sin^2(2\theta)=0.04$ and $\Delta m^2=1$ eV² (bottom). Both maps are normalized to the absolute minimum in the $\sin^2(2\theta)$ - Δm^2 parameter space.

arithm space is convenient from the computational and numerical point of view. This is one of the reason why the test statistics are typically defined as logarithm of likelihoods.

FIG. 7 shows the NLL as a function of Δm^2 and $\sin^2(2\theta)$ for two sets of pseudo-data from the toy disappearance experiment. The two sets of pseudo-data are respectively a realization of the no-signal hypothesis and a realization of a hypothesis with $\sin^2(2\theta)=0.04$ and $\Delta m^2=1$ eV². They are the same data sets used for the comparison of the performance of the statistical methods in the previous sections. Local minima at regularly-spaced Δm^2 values are present for both data sets. This feature is due to the oscillatory nature of the sought-after signal and appears in any realizations of the data.

The presence of multiple minima makes it difficult for a

minimization algorithm to converge to the absolute minimum, in particular for those algorithms relying on the derivate of the function (e.g. the algorithms known as SIMPLEX and MIGRAD in the MINUIT software package [45]). To reliably find the absolute minimum we adopt a scanning approach in which Δm^2 is increased progressively with uniform steps in the logarithmic space, each step having a length of $\log(\Delta m^2/eV^2) \lesssim 0.01$. At each Δm^2 value a minimization against $\sin^2(2\theta)$ is performed. This minimization is not problematic because, when the value of Δm^2 is fixed, the likelihood function along $\sin^2(2\theta)$ is a smooth function with a unique minimum.

The NLL for the pseudo-data generated under the no-signal hypothesis shows an other important feature: the absolute minimum does not correspond to the no-signal hypothesis. This is the case for all the realizations of the data from the toy disappearance experiment. The sought-after oscillatory signature is indeed mimicked by the statistical fluctuations between adjacent bins and the data are described always better by an oscillation hypothesis than by the no-signal hypothesis. As discussed later in Appendix D, this leads to a deformation of the test statistic probability distribution.

Appendix B: Generation of Pseudo-Data

The generation of pseudo-data is performed with Monte Carlo techniques. The experimental parameters of the two toy experiments used in this work are quoted in Section II and TABLE I. Pseudo-data for a specific hypothesis $H(X,Y) : \{\sin^2(2\theta), \Delta m^2 : \sin^2(2\theta) = X, \Delta m^2 = Y\}$ are generated according to the probability distribution of signal ($\text{PDF}_{ij}^s(X,Y)$) and background (PDF_{ij}^b) events as a function of the i -th bin in L_{rec} and j -th bin E_{rec} . To construct a set of pseudo-data, a Poisson random number is generated for each ij bin using as expectation

$$\lambda_{ij} = \tilde{N}^s(X,Y) \cdot \text{PDF}_{ij}^s(X,Y) + \tilde{N}^b \cdot \text{PDF}_{ij}^b$$

where $\tilde{N}^s(X,Y)$ is the expected number of neutrino interactions under the hypothesis $H(X,Y)$ and \tilde{N}^b is the expected number of background events. For each set of pseudo-data also the external constraints $\tilde{N}^s(X,Y)$ and \tilde{N}^b (see equation (6)) are sampled from Gaussian distributions with means $\tilde{N}^s(X,Y)$ and \tilde{N}^b and standard deviations σ^s and σ^b respectively.

N^s and N^b are nuisance parameters in our analysis and their true values $\tilde{N}^s(X,Y)$ and \tilde{N}^b are regarded as fixed during the construction of ensembles of pseudo-data. The expectation values of the nuisance parameters could also be sampled from a prior probability distribution. Ensembles generated in this way can be used to construct the probability distribution of a test statistic taking into account the systematic uncertainties on the nuisance parameters [11]. This construction leads to probability distributions that are the average over a set of models, each

model having different values of the nuisance parameters and a weight proportional to the prior probability of those specific values. This construction should be considered for T_0 . In contrast, the asymptotic probability distribution for test statistics based on the profile likelihood ratio such as T_1 and T_2 does not depend on the value of the nuisance parameters. This is expected as likelihood ratio test statistic propagates in the analysis the uncertainties on the nuisance parameters. To ease the comparison between test statistics, we generated the ensembles of pseudo-data always assuming fixed values of the nuisance parameters.

Appendix C: Hypothesis Testing and Sensitivity

The definition of the set of accepted/rejected hypotheses in this work is based on a Neyman construction in which the ordering principle is defined by the test statistic. The construction follows the steps outlined in this section.

Let T be any of the three statistics in TABLE II. T is used to test a specific hypothesis $H(X,Y) : \{\sin^2(2\theta), \Delta m^2 : \sin^2(2\theta) = X, \Delta m^2 = Y\}$ given a set of data. We will use the symbol $T_{X,Y}$ to make explicit which hypothesis is being tested. The set of hypotheses accepted or rejected by the test is defined according to how the observed value of the test statistic $T_{X,Y}^{\text{obs}}$ compares to its probability distribution against the considered hypothesis $f(T_{X,Y}|H(X,Y))$. To this purpose, the p-value is computed as:

$$p_{X,Y} = \int_{T_{X,Y}^{\text{obs}}}^{\infty} f(T_{X,Y}|H(X,Y)) dT_{X,Y}$$

The probability distributions are constructed by computing the test statistic for each data set in ensembles containing between 10^4 and 10^8 pseudo-data sets.

For each hypothesis to be tested the following steps are carried out:

1. $T_{X,Y}^{\text{obs}}$ is evaluated for the considered data set;
2. $p_{X,Y}$ is computed given $T_{X,Y}^{\text{obs}}$ and the specific probability distribution for $H(0,0)$;
3. the hypothesis is accepted if $p_{X,Y} \geq \alpha$, were α is the size of the test and defines the confidence level: C.L. = $1 - \alpha$. The hypothesis is rejected otherwise.

Two definitions of sensitivity have been used in this article: the sensitivity for limit setting that defines the set of hypotheses that would be rejected assuming the no-signal hypothesis, and the sensitivity for signal discovery that defines the set of hypotheses for which we expect to reject the no-signal hypothesis. The formal definition of these two quantities is based on the median p-value expected under certain hypotheses that can be calculated using an ensembles of pseudo-data.

The sensitivity for limit setting is defined as the set of hypotheses for which the test is expected to provide a median p-value exactly of $\alpha = 0.05$ (corresponding to 95% C.L.) assuming the data were generated from the no-signal hypothesis. To find the set of hypotheses fulfilling this requirement, the following steps are carried out for each $H(X,Y)$:

1. compute $\text{med}[T_{X,Y}|H(0,0)]$, i.e. the median value of $f(T_{X,Y}|H(0,0))$;
2. compute the p-value for $\text{med}[T_{X,Y}|H(0,0)]$, i.e.

$$p_{X,Y} = \int_{\text{med}[T_{X,Y}|H(0,0)]}^{\infty} f(T_{X,Y}|H(X,Y)) dT_{X,Y}$$

Since the set of hypotheses considered is usually discrete, finding an hypothesis that meets perfectly the condition above is not possible. The requirement is hence softened: for a given Δm^2 value, the hypotheses are tested for increasing values of $\sin^2(2\theta)$ and the first one fulfilling the condition $p_{X,Y} < 0.05$ is added to the set.

The sensitivity for signal discovery is defined as the set of hypotheses that, if true, would result in a median p-value for the no-signal hypothesis of $\alpha = 0.05$, corresponding to a median confidence level of 95%. To find the set of hypotheses fulfilling this requirement, the following steps are carried out for each $H(X,Y)$:

1. compute $\text{med}[T_{0,0}|H(X,Y)]$, i.e. the median value of $f(T_{0,0}|H(X,Y))$;
2. compute the p-value for $\text{med}[T_{0,0}|H(X,Y)]$:

$$p_{0,0} = \int_{\text{med}[T_{0,0}|H(X,Y)]}^{\infty} f(T_{0,0}|H(0,0)) dT_{0,0}$$

Similarly to the previous case, a softer requirement is typically applied when considering a discrete set of hypotheses.

Appendix D: Probability Distributions of T_2

In this section we discuss in more detail the features of the probability distributions of the test statistic T_2 when it is used to test the no-signal hypothesis on pseudo-data generated also under the no-signal hypothesis. The distributions are shown in FIG. 8 for the toy disappearance and appearance experiments, assuming a rate analysis, a shape analysis, and their combination. If the requirements of Wilks' theorem were valid, the distributions would follow a chi-square distribution with a number of free parameters of interest in the alternative hypothesis. The distributions for the rate analysis follow a half chi-square distribution with one degree of freedom $\frac{1}{2}\chi_1^2$ [43]. The tested hypothesis is at the edge of the allowed parameter range and the likelihood would be maximized by negative $\sin^2(2\theta)$ values in 50% of the cases. Since

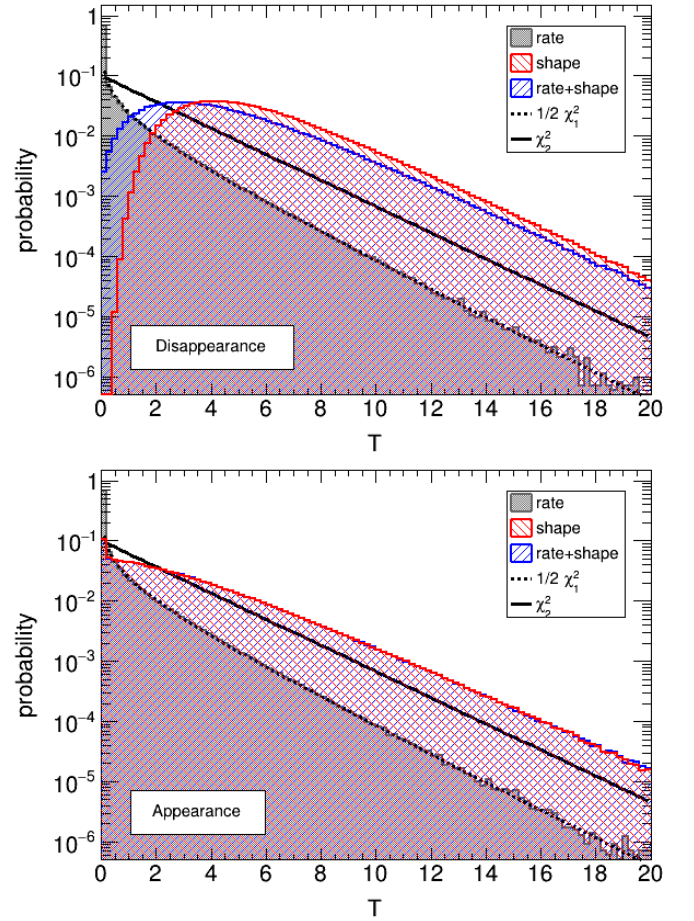


FIG. 8. Distributions of T_2 for a test of the no-signal hypothesis over an ensemble of pseudo-data generated also under the no-signal hypothesis. The distributions are shown for T_2 computed using a rate analysis, a shape analysis, and their combination.

$\sin^2(2\theta)$ is bounded to positive values, its distribution is cut-off and an accumulation of counts shows at zero. The presence of a bound prevents the estimator of $\sin^2(2\theta)$ to be normally distributed around its true value, which is one of the requirements of Wilks' theorem. When the hypothesis tested has larger $\sin^2(2\theta)$ values, Wilks' theorem requirements are met and the distribution of the test statistic tends to a one-dimensional chi-square χ_1^2 . The number of degrees of freedom is expected to be one because of the degeneracy between $\sin^2(2\theta)$ and Δm^2 with respect to the likelihood maximization.

The distributions for the shape analysis and the combination of rate and shape differ from a two-dimensional chi-square distribution χ_2^2 both for the disappearance and the appearance toy experiments. The distributions are deformed towards higher values of the test statistic and their maximum does not correspond to zero. This is due to the presence of maxima in the likelihood that do not correspond to the no-signal hypothesis assumed in the generation of the pseudo-data (see FIG. 7). The most

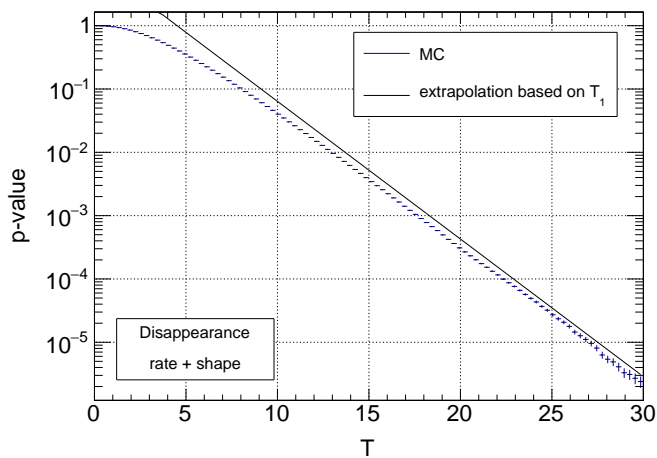


FIG. 9. global p-value computed for the no-signal hypothesis as a function of the value of the test statistic T_2 . The distribution computed from an ensemble of pseudo-data generated under the no-signal hypothesis (MC) is compared with the extrapolation based on T_1 and the procedure discussed in the text. The value of the parameters used for the extrapolation are $u_0 = 1$ and $\langle N_{u_0} \rangle = 5.603$, as estimated from 1000 sets of pseudo-data.

likely hypothesis is hence not the true one. The deviation from a chi-square function is stronger for the disappearance than for the appearance experiment. While for the disappearance the no-signal hypothesis is never the hypothesis maximizing the likelihood, in the appearance experiment this happens for $\sim 10\%$ of the pseudo-data.

When the signal is larger than the statistical fluctuations, Wilks' theorem is valid and the coverage probability for chi-square approximated distributions of the test statistic is correct (see FIG. 5). In the residual parameter space the distributions of the test statistic are deformed and a smaller coverage is indicating a larger deformation similar to the distributions of the no-signal hypothesis described above.

Appendix E: Look-Elsewhere Effect

The statistical significance associated to the observation of a sterile neutrino signal can be expressed through

the p-value computed for the no-signal hypothesis given the observed data. While T_2 provides a unique p-value for the no-signal hypothesis, T_1 provides a p-value for each tested value of Δm^2 (see FIG. 4). For this reason the p-value provided by T_1 is often called local p-value, while the p-value provided by T_2 is called global p-value. A procedure to estimate the global p-value using the local estimation has been proposed in Ref. [40] based on previous results from Davis [46]. The procedure is based on a linear correction of the minimum local p-value found:

$$p_{\text{global}} \approx \min_{\Delta m^2} p_{\text{local}} + \langle N_u \rangle$$

where $\langle N_u \rangle$ is the mean number of “upcrossings” above the level u in the range of considered Δm^2 values for a test of the no-signal hypothesis based on T_1 . Each upcrossing corresponds to a Δm^2 value for which the signal hypothesis is preferred over the no-signal hypothesis at a certain level u . The mean number of upcrossings above the level u and lower level u_0 is connected by the relationship $\langle N_u \rangle = \langle N_{u_0} \rangle e^{-(u-u_0)/2}$. $\langle N_{u_0} \rangle$ can be estimated from a small ensemble of pseudo-data. The possibility of using a small ensemble is convenient because if u_0 is small the number of upcrossings per data set becomes large.

Computing a global p-value from a local estimation would be extremely interesting for sterile neutrino searches as the local p-value construction could be performed assuming the asymptotic formula for the probability distributions of T_1 . The global p-value estimated through the correction discussed above is shown in FIG. 9 for the toy disappearance experiment. The p-value computed from T_2 using an ensemble of pseudo-data is also shown. The distributions have the same shape for large values of the test statistic but a different offset. The offset implies that the p-value extrapolated from T_1 would be overestimated by a factor of 1.4. This factor is not constant and depends on the specific experiment.

While a correction can provide accurate results in problems such as a peak search, the oscillatory nature of the signal sought-after by sterile neutrino experiments induces a correlation in the number of upcrossings. Such a correlation is due to the harmonics in equation (1) and equation (2) occurring at different values of Δm^2 . It might be possible to correct the number of upcrossings to account for the spurious occurrences but this requires additional studies.

-
- [1] C. Giunti and T. Lasserre, [arXiv:1901.08330](#).
 - [2] B. Pontecorvo, *Sov. Phys. JETP* **26**, 984 (1968).
 - [3] A. Boyarsky *et al.*, *Prog. Part. Nucl. Phys.* **104**, 1 (2019).
 - [4] A. Aguilar-Arevalo *et al.* (LSND), *Phys. Rev.* **D64**, 112007 (2001).
 - [5] G. Mention *et al.*, *Phys. Rev.* **D83**, 073006 (2011).
 - [6] C. Giunti *et al.*, *Phys. Rev.* **D86**, 113014 (2012).
 - [7] M. Dentler *et al.*, *JHEP* **08**, 010 (2018).
 - [8] G. J. Feldman and R. D. Cousins, *Phys. Rev.* **D57**, 3873 (1998).
 - [9] L. Lyons, [arXiv:1404.7395](#).
 - [10] X. Qian *et al.*, *Nucl. Instrum. Meth.* **A827**, 63 (2016).
 - [11] M. Tanabashi *et al.* (Particle Data Group), *Phys. Rev.* **D98**, 030001 (2018).
 - [12] I. Alekseev *et al.* (DANSS), *Phys. Lett.* **B787**, 56 (2018).
 - [13] Y. J. Ko *et al.* (NEOS), *Phys. Rev. Lett.* **118**, 121802 (2017).
 - [14] A. P. Serebrov *et al.* (NEUTRINO-4), *JETP Letters* **109**,

- 213 (2019).
- [15] J. Ashenfelter *et al.* (PROSPECT), *Phys. Rev. Lett.* **121**, 251802 (2018).
- [16] Y. Abreu *et al.* (SoLID), *JINST* **14**, P02014 (2019).
- [17] H. Almazn *et al.* (STEREO), *Phys. Rev. Lett.* **121**, 161801 (2018).
- [18] V. N. Gavrin *et al.*, *Phys. Part. Nucl.* **48**, 967 (2017).
- [19] G. Bellini *et al.* (Borexino), *JHEP* **08**, 038 (2013).
- [20] J. Gaffiot *et al.*, *Phys. Rev.* **D91**, 072005 (2015), 1411.6694.
- [21] S. Ajimura *et al.*, (2017), [arXiv:1705.08629](https://arxiv.org/abs/1705.08629).
- [22] A. A. Aguilar-Arevalo *et al.* (MiniBooNE), *Phys. Rev. Lett.* **121**, 221801 (2018).
- [23] M. Antonello *et al.* (MicroBooNE, LAr1-ND, ICARUS-WA104), (2015), [arXiv:1503.01520](https://arxiv.org/abs/1503.01520).
- [24] F. P. An *et al.* (Daya Bay), *Phys. Rev. Lett.* **117**, 151802 (2016).
- [25] D. Hellwig and T. Matsubara (Double Chooz), *J. Phys. Conf. Ser.* **888**, 012133 (2017).
- [26] I. S. Yeo (RENO), *J. Phys. Conf. Ser.* **888**, 012139 (2017).
- [27] P. Adamson *et al.* (MINOS+), *Phys. Rev. Lett.* **122**, 091803 (2019).
- [28] P. Adamson *et al.* (NOvA), *Phys. Rev.* **D96**, 072006 (2017).
- [29] M. G. Aartsen *et al.* (IceCube), *Phys. Rev.* **D95**, 112002 (2017).
- [30] N. Aghanim *et al.* (Planck), (2018), [arXiv:1807.06209](https://arxiv.org/abs/1807.06209) [[astro-ph.CO](https://arxiv.org/abs/1807.06209)].
- [31] J. Angrik *et al.* (KATRIN), “KATRIN Design Report,” (2004), Wissenschaftliche Berichte, FZ Karlsruhe 7090.
- [32] L. Gastaldo, C. Giunti, and E. M. Zavatin, *JHEP* **06**, 061 (2016).
- [33] F. Beaujean *et al.*, *Phys. Rev.* **D83**, 012004 (2011).
- [34] G. Casella and R. L. Berger, *Statistical inference* (Thomson Learning, Australia Pacific Grove, CA, 2002).
- [35] G. Cowan, in *Proceedings, 69th Scottish Universities Summer School in Physics : LHC Phenomenology (SUSSP69): St. Andrews, Scotland, August 19-September 1, 2012* (2013) pp. 321–355.
- [36] G. Cowan, K. Cranmer, E. Gross, and O. Vitells, *Eur. Phys. J.* **C71**, 1554 (2011), [Erratum: *Eur. Phys. J.* **C73**, 2501(2013)].
- [37] S. S. Wilks, *Ann. Math. Statist.* **9**, 60 (1938).
- [38] R. D. Cousins and V. L. Highland, *Nucl. Instrum. Meth.* **A320**, 331 (1992).
- [39] *Procedure for the LHC Higgs boson search combination in Summer 2011*, Tech. Rep. CMS-NOTE-2011-005. ATLAS-PHYS-PUB-2011-11 (CERN, Geneva, 2011).
- [40] E. Gross and O. Vitells, *Eur. Phys. J.* **C70**, 525 (2010).
- [41] G. Ranucci, *Nucl. Instrum. Meth.* **A661**, 77 (2012).
- [42] A. Stuart and K. Ord, *Kendall’s Advanced Theory of Statistics: Volume 1: Distribution Theory*, Kendall’s Advanced Theory of Statistics No. v. 1; v. 1994 (Wiley, 2009).
- [43] H. Chernoff, *Ann. Math. Stat.* **25**, 573 (1954).
- [44] A. L. Read, *Modified frequentist analysis of search results (the CL_s method)*, Tech. Rep. CERN-OPEN-2000-205 (2000).
- [45] F. James and M. Roos, *Comput. Phys. Commun.* **10**, 343 (1975).
- [46] R. B. Davies, *Biometrika* **74**, 33 (1987).